University of Brasília
Faculty of Technology
Department of Electrical Engineering

Instrumentation of a Quarter-Vehicle Suspension Test Bench

Matheus Amaral Siqueira
Rodrigo Alves de Araujo

FINAL REPORT

CONTROL AND AUTOMATION ENGINEERING

Brasília
2023

University of Brasília
Faculty of Technology
Department of Electrical Engineering

Instrumentation of a Quarter-Vehicle Suspension Test Bench

Matheus Amaral Siqueira
Rodrigo Alves de Araujo

Final report submitted as a partial requirement for obtaining the Bachelor's degree in Control and Automation Engineering.

Orientador: Prof. Dr. Evandro Leonardo Silva Teixeira
Coorientador: Prof. Dr. Eugênio Libório Feitosa Fortaleza

Brasília
2023

Siqueira, Matheus Amaral.
S618i Instrumentation of a Quarter-Vehicle Suspension Test Bench / Matheus Amaral Siqueira; Rodrigo Alves de Araujo; orientador Evandro Leonardo Silva Teixeira; coorientador Eugênio Libório Feitosa Fortaleza. -- Brasília, 2023.
88 p.

Final report em Control and Automation Engineering -- University of Brasília, 2023.

1. Suspensão. 2. Instrumentação. 3. LabVIEW. 4. Controle. I. Araujo, Rodrigo Alves de. II. Teixeira, Evandro Leonardo Silva, orient. III. Fortaleza, Eugênio Libório Feitosa, coorient. IV. Título

University of Brasília
Faculty of Technology
Department of Electrical Engineering

Instrumentation of a Quarter-Vehicle Suspension Test Bench

Matheus Amaral Siqueira
Rodrigo Alves de Araujo

Final report submitted as a partial requirement for obtaining the Bachelor's degree in Control and Automation Engineering.

Approved report. Brasília, February 16 th, 2023 :

Prof. Dr. Evandro Leonardo Silva Teixeira, UnB/FGA
Orientador

Prof. Dr. Eugênio Libório Feitosa Fortaleza, UnB/FT/ENM
Coorientador

Prof. Msc. Rafael Rodrigues da Silva, UnB/FGA
Examinador

Prof. Dr. André Murilo de Almeida Pinto, UnB/FGA
Examinador

Brasília
2023

I dedicate this work to my parents, Mauro and Dilma,
and also to my younger brother Marcos,
who always supported me in all possible ways
to break through the barriers to the knowledge
to reach my dreams and evolve as a human being.

Matheus Amaral Siqueira

I dedicate this work to my parents, Geane and Jairo,
and also to my siblings Ana Beatriz and Wallas,
for your support and encouragement in this phase of life.
Your motivation served as an impulse to keep me
on challenging stages and overcome the adversities.

Rodrigo Alves de Araujo

Acknowledgements

I thank to Fundação de Apoio e Pesquisa (Fundep) for bringing the university closer to the automotive industry. To my advisor Prof. Dr. Evandro Teixeira and co-advisor Prof. Dr. Eugênio Libório, who managed to guide us with flexibility and shared their knowledge in order to assist us to carry out this work. To all the other professors, especially Prof. Dr. Alessandro Borges, who also helped us due to the synergic nature of this work.

I also thank the competition team Piratas do Cerrado, who provided my first experience with embedded electronics in my career. To Origem Motos, for introducing me to the automotive industry and for giving me the opportunity to work developing technology in a company with a huge diversity of people. To the Student Assistance, for aiding me to remain at the university more focused my energy on my career.

Lastly, I thank all my friends that I made during this journey for their respect, talking and advice. Especially to Rodrigo Alves, who worked with me on this work for the magnificent partnership.

Matheus Amaral Siqueira

I firstly thank God for life, dreams, and faith. I am entirely grateful to supervisor Prof. Dr. Evandro Teixeira and co-supervisor Prof. Dr. Eugênio Fortaleza, who were always willing to listen to the proposals and advised the better ways for decisions. To other professors who were essential in the rig implementation, Prof. Dr. Alessandro Borges, Prof. Dra. Maria Alzira, and Prof. Dr. André Murilo. I also thank all the technicians and employees who take care functioning and safety of rooms and laboratories at the University of Brasilia properly.

To FGR, the electric Formula SAE team, for introducing me to the structural and electronics automotive environment. I also thank Mega-X Engineering and Akvofluo Engineering and Technology. Dealing with challenges, project decisions, and deadlines were fundamental to my personal development as an engineer.

Finally, to the friendship of the comrades that I made over the years, especially my work partner Matheus Amaral, with who I shared challenges, duties, responsibilities, and learning throughout the entire research.

Rodrigo Alves de Araujo

"Success represents the 1% of your work
which results from the 99% that is called failure.
Instead of being afraid of the challenge and failure,
be afraid of avoiding the challenge and doing nothing."
(Soichiro Honda)

Abstract

The present work aims at the instrumentation of a test bench for the suspension of a quarter-car. To achieve this, the work was divided into two stages. The first one delimits the design of the project, starting with the study of standards and commercial benches to define parameters to be monitored. From this, it was made an analysis of the available bench, allowing to define the instrumentation to be integrated into it, including sensors and security mechanisms. While the second stage consists of continuing the previous execution project, adding improvements to the embedded system, integration between sensors, data acquisition, and actuators. Furthermore, there is the use of a proportional valve controller already developed in previous works. Still, in the second stage, it was proposed an encapsulation for the instrumentation that holds acquisition modules, sources, and connections, minimizing direct contact with the hardware and bringing the user focus on setting up the test parameters. For this reason, a human-machine interface was developed to allow the configuration of tests through the signal applied to a proportional valve and reproduces the road excitation on the bench.

Keywords: Suspension. Instrumentation. LabVIEW. Control.

Resumo

O presente trabalho visa a instrumentação de uma bancada de testes da suspensão de um quarto de veículo. Para isso, o trabalho foi dividido em duas etapas. A primeira delimita-se à concepção do projeto, inicializando com o estudo de normas e bancadas comerciais para definir parâmetros a serem monitorados. A partir disso, tem-se a análise da bancada disponível, permitindo definir a instrumentação a ser integrada à bancada, incluindo sensores e mecanismos de segurança. Enquanto a segunda etapa consistiu em dar continuidade ao trabalho por meio da execução do projeto, aprimoramento da eletrônica embarcada, integração de sensores, aquisição de dados e atuadores. Além disso, tem-se a utilização de um controlador da válvula proporcional já desenvolvido em trabalhos anteriores. Ainda na segunda etapa, foi proposto um encapsulamento para a instrumentação que abriga módulos de aquisição, fontes e conexões, minimizando contato direto com o hardware e trazendo para o usuário foco na configuração de parâmetros do seu teste. Assim, desenvolveu-se uma interface homem-máquina que permite a configuração de testes por meio do sinal aplicado válvula proporcional e reproduz na bancada a excitação de pista.

Palavras-chave: Suspensão. Instrumentação. LabVIEW. Controle.

List of Figures

List of Tables

List of abbreviations and acronyms

3D	3 dimensions	62
A/D	Analog to Digital Converter	44
ABS	Acrylonitrile Butadiene Styrene	62
CJC	Cold-junction compensation	59
D/A	Digital to Analog Converter	44
ADC	Analog Digital Converter	51
DOF	Degree Of Freedom	24
FFT	Fast Fourier Transform	73
FGA	Faculty of Gama	26
HPIS	High Impact Polystyrene	62
LED	Light Emitting Diode	32
PID	Proportional Integral and Derivative	24
RMS	Root Mean Square	25
SMRC	Sliding Mode Reference Conditioning	24
SPD	Surge Protective Device	61

List of symbols

c(t)	Controlled signal	43
e(t)	Signal of error	43
r(t)	Reference signal	43
u(t)	Signal of Control action	43
y(t)	Output signal measured by sensor	43

Contents

1 Introduction

The automobile can be divided into several systems as exposed in (HASBOLLAH, 2021), which work together to perform a particular behavior to manage vehicle dynamics to take people from one point to another safely and quickly.

Considering that, there are three main systems that actuate in the vehicle's dynamics. The first is the powertrain system, which acts as a propulsion source and defines how fast the car moves, handling with the engine, and transmission of power to the tires. The second is the braking system, which aims to develop a fast-responding reliable security mechanism to stop the vehicle. The last is the suspension system, being one of the objects of interest in this work, it is applied to lateral and vertical motions control of the vehicle in order to deliver a proper dynamic response when the vehicle accelerates, brakes, or corners, dictating how comfortable is to its users.

Handling with translational and rotational movements of the vehicle, the suspension system improves the road holding, providing the car the ability to accelerate, brake, and corner without the tires losing contact with the road through the mitigation of the load variation of the tires. In addition, provide ride quality, ensuring comfort to the occupants of the vehicle and minimizing the vertical acceleration transmitted to the chassis. And last, support the vehicle's static weight, maintaining the suspension deflection at small values.

Given this, the suspension system performs an essential role in modern vehicles, and comprehending how its components influence the car's behavior is a valuable step to attend to the increasing advancements in automotive suspension systems in the next years (RESEARCH, 2021). Thus, to guarantee its functional purposes, some methodologies can be applied. Therefore, the evaluation process can be carried out through outdoor and indoor tests.

The outdoor tests validate the indoor tests and support the experiments as close as to the real application environment, in order to acquire external influences and interruptions. In this way, whether the results are approximate to the indoor tests, it is possible to confirm that the indoor tests reproduce similar results as the outdoor tests. The indoor tests are focusing on durability and fatigue analyzes, on the other hand, the outdoor tests are required because it has data reliability and large range of real situations, considering the vertical and horizontal suspension dynamics, as said by (GAGLIANO et al., 2012). Moreover, the (VETTURI; MAGALINI, 2002) followed the methodology of evaluating the road profile and obtained good agreement between reproduced on indoor simulation tests and observed on outdoor results, that is for vertical accelerations and wheel-body displacement.

As for the indoor tests, they must also be considered, once they can provide valuable

results allowing researchers of automotive technology to validate models in the initial and intermediary development stages in their laboratories. However, they still have faced challenges to evaluate their models due to the intrinsic constraints of the automotive industry, mainly costs and complexity of the available technologies, such as 4-post, 7-post, and 8-post rigs (LANGDON, 2007), (SALEM, 2018).

Thus, a quarter-vehicle test rig is proposed as a tool to validate the behavior of a suspension for given values of suspension damping and stiffness as well as its geometry through an experimental manner that allows the designer to obtain suspension performance in terms of ride quality, road holding, and the suspension deflection. Furthermore, improving the process of design and choice of the main components of the suspension system.

The usage of simulations on first steps before actual dynamic tests is the reality of suspension development. The well-designed projects result in a smaller source of mistakes in the production phase. Nowadays, there are some enterprises specialized in suspension modeling such as (MODELON, 2023) and (COLLIMATOR, 2023), which are focused on the vehicle dynamics library.

A time ago the 4, 7, and 8-post rigs were explored mainly by motorsport teams. Nevertheless, the manufacturers have been invested in research and technology for their projects, which include the usage of 7 and 8 post rigs to simulate lateral force, and downforce acceleration. Further, second as (KW, 2023) the other benefits of the 7-post rig are testing the vehicle that is not ready to drive, data analysis in Matlab or Excel environment, and the principal is the capability to optimization of the parameters as minimum tire contact forces, dynamic vehicle level, anti-sway bar tests, the influence of different types of tires and its pressures, and the tire stiffness.

For the (SERVOTEST, 2023) the 7-post rig shows advantages in modeling the vehicle behavior in the Simulink environment as enhancing the dynamic responses. For instance, setting up the custom aerodynamic maps and then configuring the aero loader at any selected moment, promotes better knowledge of the dynamics limits of the vehicle without contact with the actual road and decreases the risk of damage to the vehicle body.

The (JOIE, 2023) says that a suspension 7-post rig is used to tune the suspension dampers. The goal is to minimize the deviation of the contact between the tire and road profile, and additionally, improve the aerodynamics as the pitch moves. However, the 7-post rig can not asset anti-dive, anti-squat, and measure the roll center forces, because the suspension rig movement just applies vertical load, without breaking, and cornering. Note that, outdoor tests are necessary to validate the dynamical characteristics of the vehicle, and they can not be evaluated in indoor tests.

Hence, this work aims to improve a quarter-car suspension test rig, refining the instrumentation, standardizing cables and connectors, and implementing a human-machine

interface using graphical programming through Labview. The final test rig might be easy to set up, handle, and maintain for the final user.

1.1 Aim and Objectives

This report aims to analyze and instrument a quarter-car suspension test rig. The main objectives are listed as follows:

1) To analyze standardized methodologies and literature in order to establish the functional requirements of the bench;
2) To organize and enclosure its electrical system to improve the measurement system robustness;
3) To provide a simplified set-up capable of ensuring to the user an easy-to-prepare data monitoring system, carrying out tests as well as repairing in case of failures.
4) To develop an user interface that allows monitoring the real-time suspension data performance and storing data for report generation and later analyses.

1.2 Report Organization

- Chapter 1: Introduction

The introduction aims to present the purpose of the suspension system in vehicles, and how it impacts on the daily life of drivers and passengers.

- Chapter 2: Literature Review

This chapter is a review of the standard, theoretical principles, and technical aspects of the measurement systems and actuator requirements.

- Chapter 3: Project Development

This chapter describes how the parameters are monitored and furthermore about the functional requirements, the proposed solution, and the input and output channels configuration as well. Finally, it is described the control actuation and the electrical system.

- Chapter 4: Software Development

Treatment of the software development and the code aspects. Besides, it presents how the software is organized.

- Chapter 5: Results

This section summarizes the results of the test bench. As well as, it is shown the hardware limitations.

- Chapter 6: Conclusion

This section describes the entire project. Whether the solution performance is satisfactory and if the solution meets the initial requirements.

- Chapters 7: Future Prospects

The chapter describes the points that can be reached and improved. This section is important because deals with the way of a quarter-vehicle test bench are taken in.

2 Literature Review

2.1 Suspension System

The suspension system can be characterized as a mechanism that absorbs kinetic energy from bumps and other irregularities on the road and dissipates it in form of heat. As a result, the car becomes able to offer a good user experience by reducing the effects of the shocks on the car body and, simultaneously, keeping its stability, concerning the safety of the occupants of the vehicle. In essence, a suspension system consists of three subsystems (RILL, 2011). The first is the guiding elements, such as control arms, links, and leaf springs. The second is the force elements, which are represented by the springs, shock absorbers, stabilizer bar, and bushings. Last but not least, there are the tires.

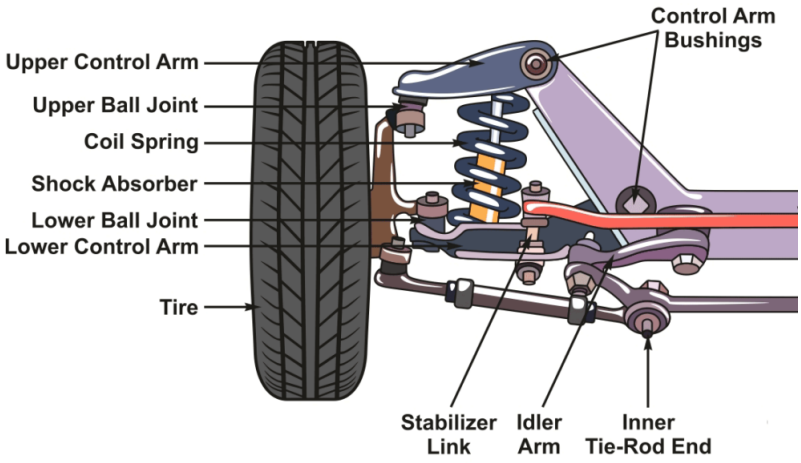

Figure 1 – Suspension system (TRUCK, 2020).

From Figure 1 (TRUCK, 2020), it can be seen how the components in the suspension subsystems are integrated together. Taking the main components, their functions can be listed as follows:

- *Shock Absorber* - It performs an important role, because it dampers oscillations from the spring and dissipates it in form of heat, increasing grip and providing a comfortable ride to its occupants (WULING, 2021).
- *Springs* - They absorb energy from road shocks avoiding this to be transferred to the vehicle body. When the car passes over a bump, the spring is compressed storing energy. Then, during its extension cycle, the stored energy is transformed into heat by the dampers (WULING, 2021).

- *Control arms* - They are responsible for attaching the wheel hubs to the vehicle frame. Besides that, they keep wheel alignment, preventing the tires from exerting lateral movements while allowing vertical movements as the wheels move up or down.
- *Tires* - In brief, they are air springs that support the vehicle load during dynamic and static situations, and also transmit the braking or acceleration forces to the road in order to guide the vehicle along a specific path demanded by the driver (MICHELIN, 2022).

2.2 Road Excitation

The dynamic behavior of the vehicle at specific terrains can change drastically. As a result, it affects the experience of the driver and the passengers about how appropriate the car appears to be, considering comfort and safety. In that way, to create models of road excitation that approach to real cases, it is useful to generate road profiles that can be used as inputs for testing the suspensions and analyzing the performance along a given road.

To represent the irregularities of the road, a sine wave model can be used to generate a periodic road excitation defined as below (RILL, 2011).

$$z_R(s) = Asin(\Omega s) \tag{2.1}$$

where z_R is the road height for a single track road model, in which $z_R = z_1 = z_2$, as in Figure 2, Ω is the wave number, s the path parameter, and A the amplitude.

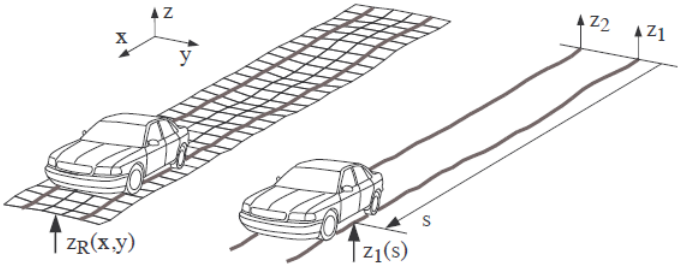

Figure 2 – Parallel track road model (RILL, 2011)

.

Assuming that the vehicle is running at a constant speed, it can be noted that its instaneous position is given by $s = v_0 t$, and with null initial velocity at $t = 0$. Then, defining wavelength as in Equation 2.2.

$$L = \frac{2\pi}{\Omega} \tag{2.2}$$

Taking Ωs from Equation 2.1

$$\Omega s = \frac{2\pi}{L} s = \frac{2\pi}{L} v_0 t = \omega t \tag{2.3}$$

thus, knowing that excitation frequency f is expressed as in Equation 2.4.

$$f = \frac{\omega}{2\pi} \tag{2.4}$$

Finally the excitation frequency can be rewritten as follows:

$$f = \frac{2\pi \frac{v_0}{L}}{2\pi} = \frac{v_0}{L} \tag{2.5}$$

In addition, it can be noted the rigid vibrations range from 0.5Hz to 15Hz (RILL, 2011). That way, the limits for excitation frequency must be defined considering v_{min} (minimum velocity) and v_{max} (maximum velocity) of the vehicle, making $v_{min} = 0.5L$ and $v_{max} = 15L$, as expressed by Equation 2.6.

$$\frac{v_{min}}{L} \leq \frac{v_0}{L} \leq \frac{v_{max}}{L} \tag{2.6}$$

2.3 Comfort Standard

Vibration is one of the greatest enemies of engineering, because it can reduce machinery life and also, at excessive levels, trigger symptoms in humans such as motion sickness and discomfort (GRIFFIN, 1990). As a result, comfort is one of the main requirements that a car must guarantee to its occupants. And to ensure that the vehicle produces safe levels to its users, standards are used.

ISO 2631-1 defines measuring methods of periodic, random and transient mechanical vibration, which is transmitted to the whole body. To achieve that, the acceleration parameter is monitored with an appropriate measurement system, and analyzed utilizing frequency weighting of the r.m.s. acceleration through the equation 2.7. In order to do that, the crest factor must be less or equal than 9. Notice that, if the crest factor is greater than 9, it may not be enough to evaluate the acceleration levels of the body and then alternative methods should be applied.

$$a_w = \left[\frac{1}{T} \int_0^T a_w^2(t)\, dt \right]^{\frac{1}{2}} \tag{2.7}$$

where, a_w is the weighted acceleration in (m/s^2), and T is the measurement duration (s).

Even though ISO 2631-1 does not establish limits to vibration values, Table 1 can be used to indicate possible reactions to specific ranges due the exposure to vibration in public transport. However, the effects of these values can be investigated in isolation, as the reactions can vary from passenger to passenger.

Table 1 – Comfort Perception

Acceleration m/s^2	**Consequence**
Less than 0.315	not uncomfortable
Between 0.315 and 0.63	little uncomfortable
Between 0.5 and 1	a fairly uncomfortable
Between 0.8 and 1.6	uncomfortable
Between 1.25 and 2.5	very uncomfortable
Greater than 2	extremely uncomfortable

Source: ISO 2631-1.

2.4 State of Art

The work of (LEÓN-VARGAS; GARELLI; ZAPATEIRO, 2017), was based on limiting vertical acceleration for ride comfort in active suspension systems. They studied control strategies for active suspension systems using a PID controller as the main control for suspension deflection, and also the car body vertical acceleration as the complementary source of control for the sliding mode reference conditioning (SMRC) algorithm investigated. The half-car model was adopted and it was evaluated with a bump excitation. The authors analyzed the controller with the SMRC algorithm and PID controller without SMRC, as well as the passive suspension system results.

The bump is used to evaluate the 4-DOF system response as well as its disturbances. They consider the disturbance in the second wheel as a delay from the signal in the first wheel. At a low frequency, the bump disturbances are more attenuated to the PID without SMRC. The results show that the PID controller + SMRC algorithm is prone to not uncomfortable with the ISO standard, while the PID controller response is a little uncomfortable and fairly uncomfortable for uncontrolled. Also, the R.M.S vertical acceleration is 54,3% and 44,4% less concerning uncontrolled and PID control, respectively.

(MITRA et al., 2015) proposed a design experiment based on the optimization of a quarter-car suspension test rig. They evaluated ride comfort (RC) and road holding (RH) by changing some variables like angular velocity, tire pressure, camber and toe adjustment, spring stiffness, damper coefficient, and sprung mass. They used a statistical regression approach, to analyze R-sq (Predicted coefficient) and R-sq (Adjusted coefficient), to select the best combination of values that result in optimum road holding and ride comfort to the suspension system.

The author's focus is on the correlation of data obtained in experiments, to find the best prediction model that represents the physical model. They used a statistical ANOVA technique to measure the R-squared values that represent the RC and RH of the physical model. The main objective is to maximize the RC and RH, so that, they aimed to minimize both vertical acceleration and displacement of the center wheel and chassis.

Thus, they analyze the influence of the whole parameters individually as well as their interactions. The high value of correlation between physical and predicted variables results in a quarter-car suspension optimizer tool, which means building suspension models more precisely as the engineer wonders.

(AL-ZUGHAIBI; XUE; GROSVENOR, 2019) investigated the passive suspension system. The main bullet of their study is to consider the non-linear friction forces and consider inclined a quarter car test rig. They compared the theory and experimental procedures of a quarter-car passive suspension system. Despite the new sophisticated solutions for suspension systems as semi-active and active known, the passive is used more often, in face of its simplicity and costs. The authors chose a PI controller for a hydraulic servo valve that has been used as a road input closed loop. It was necessary to map the dynamic response of Electro-hydraulic servo systems because there is high nonlinearity in oil leakage, oil temperature, dead zone response, and other inherent characteristics.

The authors compare a C++ simulation to an experimental ramp plus step function as road input. For that, they used 3 values for amplitudes (30, 50, and 70 mm) values for the distance between the mid to top of the actuator. They were worried in validated the viscous damper and spring stiffness, as well as measuring how important is to consider the non-linearities of friction forces, in addition, consider an inclined quarter car test bench. Finally, the proposal is to experiment with their model also in a half and full car model, because the effects studied in the real world are so tiny.

(SALEM, 2018) investigated a non-linear quarter-car suspension model, and also compared its model to a linear spring. The author proposed designing a new type of suspension and inserting it into the experimental setup. This is another study that involves an optimum choice for parameters such as spring stiffness and damper coefficient. The author used an automated genetic algorithm to find the best combination of the parameters taking into account a vertical RMS acceleration classified by ISO 2631, for his analysis the 1-DOF model was sufficient.

He proposed different spring geometries such as cylindrical and conical, and also experimented with their linear and nonlinear behaviors. These linear and nonlinear models were proofed with static and variable sprung mass, and after with static and variable velocity. The author integrated the nonlinear spring into the suspension and observed a decrease in the amplitude of the sprung mass by 50% to 60%. Furthermore, using the genetic algorithm and obtaining new parameters for the designing spring the amplitude would diminish from

60% up to 90%.

The author highlighted the importance of improvement of a passive suspension system just by doing experiments modifying the damper coefficients and spring stiffness parameters, by changing its geometry. He investigated a range of velocity and amplitude of bumps and also achieved the enhancement of a suspension system without an external energy source as different from a semi and full-active suspension setup.

The current test bench is available in the laboratory of the Faculty of Gama (FGA) where previously students work on a quarter-car suspension test bench, whereas the proposal was to study the fatigue of shock absorbers, as well as the vertical acceleration of a wheel. The suspension rig does not have much documentation, and the sensors that had been used before does not available anymore. In face of it, we had to use other sensors, as well as calibrate each one.

The older version of the test rig has LabVIEW software that handles inputs for sensors and the output for the pneumatic actuator. Therefore, we find some disagreements in the values of gains used in the PID controller and the recommended value of frequency of sinusoidal input signal. There is information that advises that if the user desires a quick response from the system, the value of the derived gain must be increased. On the other hand, whether the user wants to increase the precision of the system then the value of integral gain must be increased. But the previous researcher did not leave a document that explain how the PID gains were calculated.

In face of this gap of information, we ran the current LabVIEW code only for introduction in the suspension test rig environment, but we had to develop our own code, considering new sensors. Figure 3 shows the test bench before we start to develop our research.

2.5 Suspension Test Rigs

There are some types of test benches that can be used to evaluate suspension system performance to ensure a good trade-off between comfort and safety before integrating it into a prototype vehicle. Besides that, they are capable of reducing cost, time development, and risks in the earlier stages of the project (MTS, 2011). For instance, utilizing a full car model, seven-post rigs help engineers to comprehend the vehicle response through sine sweep tests, to obtain the its behavior to certain track profiles and from them to optimize suspension components (ENGINEERING, 2018).

However, as this technology is more restricted to motorsport teams, another type based on the quarter-car model, the quarter-car test rig can be also applied to obtain suspension parameters in terms of ride comfort and road holding. For instance, (KOCH et al., 2010) designed a quarter-car test rig to investigate a nonlinear model suspension system's

Figure 3 – The initial state of test bench

Figure 4 – 7-post rig (ARC, 2022)

.

behavior and provide experimental validation of active suspension's controllers using real road profile excitation. While (PATHARE, 2014), developed a test rig aiming to evaluate the passive suspension performance on a class C road. Thus, it can be concluded that there are many researches applying quarter-car analyses with the purpose of evaluating their models to improve suspension systems.

In synthesis, it can be realized that a quarter-car test rig can offer good capability of testing different suspensions and therefore, considering the test requirements, a quarter-car rig must be considered due to its greater manufacturability, less complexity, and cost compared to other models.

2.6 The Quarter-Car Vehicle Model

The diagram of Figure 5 illustrates the quarter-car model for a passive suspension system as proposed by (RAJAMANI, 2006). Where m_s represents the sprung mass, that is the weight supported by the suspension of the vehicle, while m_u is the unsprung mass is the weight that is not supported by the suspension system, including wheels, tires, brakes, etc. In addition, b_s is the damping coefficient of the suspension system damper, and k_s is the stiffness of the suspension spring. This model also includes the stiffness of the tire which is given by k_t, while the tire damping b_t is assumed to be negligible.

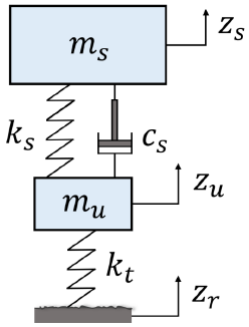

Figure 5 – Diagram of a quarter vehicle model

.

Analyzing the system in Figure 5 and applying the second Newton's Law, we obtain the following dynamic equations:

$$m_s\ddot{z}_s + c_s(\dot{z}_s - \dot{z}_u) + k_s(z_s - z_u) = 0 \tag{2.8}$$

$$m_u\ddot{z}_u + k_t(z_u - z_r) - c_s(\dot{z}_s - \dot{z}_u) - k_s(z_s - z_u) = 0 \tag{2.9}$$

According to (NISE, 2011), a system can be represented in state space as:

$$\begin{aligned} \dot{x}(t) &= Ax(t) + Bu(t) \\ y(t) &= Cx(t) + Du(t) \end{aligned} \tag{2.10}$$

in which, $\dot{x}(t)$ is the first derivative of the state vector, $x(t)$ is the state vector, $u(t)$ is the input vector, $y(t)$ is the output vector. As for the matrices, A is the state space matrix, B is the input matrix, C is the output matrix, D is the direct transmission matrix. Then, picking out the state variables as follow:

$x_1 = z_s - z_u$ is the suspension deflection

$x_2 = \dot{z}_s$ is the sprung mass absolute velocity

$x_3 = z_u - z_r$ is the wheel deflection

$x_4 = \dot{z}_u$ is the unsprung mass absolute velocity

Assuming the input system as $\dot{z}_r$, due the excitation of the road profile z_r then, in state space the system represented by Equations 2.8 and 2.9, can be rewritten as bellow:

$$\begin{bmatrix} \dot{x}_1 \\ \dot{x}_2 \\ \dot{x}_3 \\ \dot{x}_4 \end{bmatrix} = \begin{bmatrix} 0 & 1 & 0 & -1 \\ \frac{-k_s}{m_s} & \frac{-c_s}{m_s} & 0 & \frac{c_s}{m_s} \\ 0 & 0 & 0 & 1 \\ \frac{k_s}{m_u} & \frac{c_s}{m_u} & \frac{-k_t}{m_u} & \frac{-c_s}{m_u} \end{bmatrix} \begin{bmatrix} x_1 \\ x_2 \\ x_3 \\ x_4 \end{bmatrix} + \begin{bmatrix} 0 \\ 0 \\ -1 \\ 0 \end{bmatrix} \dot{z}_r$$

$$y(t) = \begin{bmatrix} 1 & 0 & 0 & 0 \\ \frac{-k_s}{m_s} & \frac{-c_s}{m_s} & 0 & \frac{c_s}{m_s} \\ 0 & 0 & 1 & 0 \\ \frac{k_s}{m_u} & \frac{c_s}{m_u} & \frac{-k_t}{m_u} & \frac{-c_s}{m_u} \end{bmatrix} \begin{bmatrix} x_1 \\ x_2 \\ x_3 \\ x_4 \end{bmatrix} \tag{2.11}$$

where Equation 2.11 allows us to evaluate the performance parameters of the suspension system.

2.6.1 Monitored Parameters

Taking all functionalities approached in Section 2.5, in quarter-car test rigs the following parameters should be monitored:

- *Sprung mass acceleration*: It is the vertical acceleration transmitted to the vehicle chassis. It is one most of the most important parameters because it can provide quantitative value for comfort indication.
- *Suspension travel*: It is given by displacement between the sprung mass and to unsprung mass. For being related to the spring deflection it can be used to assess the space required by the suspension spring (HAMED et al., 2014).
- *Tire deflection*: The relative displacement between the unsprung mass to the road. This parameter can be used to quantify the providing of a suspension (RAJAMANI, 2006), it also measures how well the car can accelerate, brake, and corner without the tires losing contact with the road.
- *Wheel position*: The displacement of the wheel is another necessary parameter to monitor due to the displacement control demanded by the actuator keeping it inside the displacement range.

- *Wheel load*: It is the input force applied by an actuator to excite the tire. On another side, at the same time, it provides a mechanism for monitoring the vertical loads maintaining the actuator inside the limits of the allowed working force.
- *Temperature*: it was not found as a variable of being monitored during tests in a quarter car test rig, but it is known that given some temperature conditions, this parameter can influence the shock absorber damping coefficient (PAVLOV, 2017).

2.7 Measurement Systems

2.7.1 Displacement Measurement

2.7.1.1 Potentiometric Ruler

The suspension deflection is a valuable parameter as explained in subsection 2.6.1 and can be obtained through a potentiometer or an LVDT (linear variable differential transformer) (DIXON, 2007). Potentiometers are composed by cylindrical resistive material, such as carbon, cerment, cermet, wire-wound, and conductive plastic films, in which the resistance is linearly related to the rectilinear variation of position (BENTLEY, 2005).

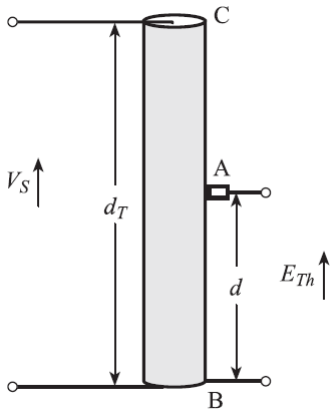

Figure 6 – Linear displacement transducer (BENTLEY, 2005)

.

Applying the Kirchhoff's voltage law (IRWIN; NELMS, 2011) in Figure 6 (BENTLEY, 2005):

$$V_s = \upsilon_{R_{CB}} \tag{2.12}$$

and,

$$E_{th} = \upsilon_{R_{AB}} \tag{2.13}$$

then, from Equation 2.12,V_s represents the voltage source, $\upsilon_{R_{CB}}$ the voltage across CB, and R_{CB} the resistance across CB being also denoted as the total resistance of the poten-

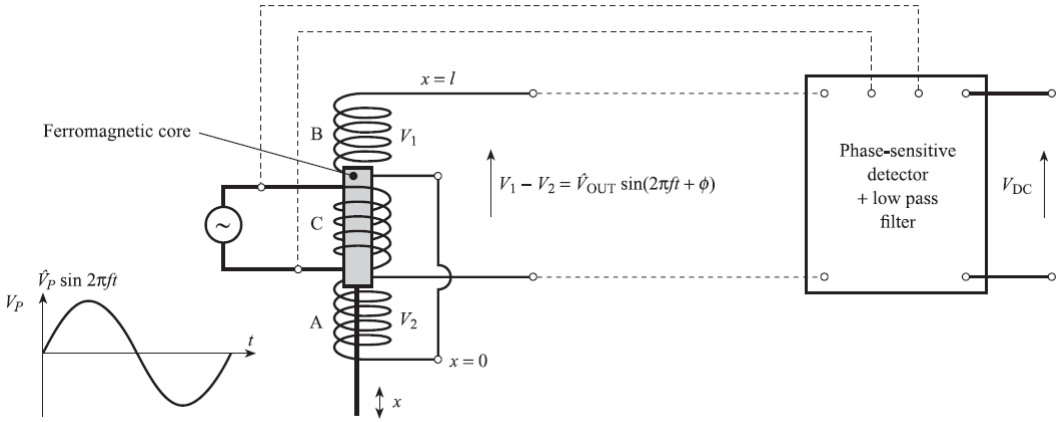

Figure 7 – LVDT and connections to phase-sensitive detector (BENTLEY, 2005).

tiometer R_p. While the output voltage E_{th} is given by the voltage drop due to changes of the fractional resistence R_{AB}, defined as $R_p \frac{d}{d_T}$. Thus, making Equation 2.13 divided by Equation 2.12:

$$E_{th} = V_s \frac{d}{d_T} = V_s x \tag{2.14}$$

From Equation 2.14 we have a linear relation between output voltage E_{th} and the fractional displacement x. That way, the resistance between A and B is proportional to the distance traveled by the wiper d.

According to (BENTLEY, 2005), LVDTs are based on the working principle of a transformer with a single primary winding, two secondary windings connected in series opposition with the ends of the primary winding and a moving ferromagnetic nucleus inside the set of windings. As illustrated in Figure 7, the primary winding is directly connected to an a.c voltage source, and as the ferromagnetic core moves a variation in mutual inductance between the primary and the secondaries windings occurs producing an a.c. output voltage given by:

$$V1 - V2 = \hat{V}_{OUT} sin(2\pi f t + \Phi) \tag{2.15}$$

after that, the output signal from Equation 2.15 is sent to a *phase sensitive detector or demodulator*, which converts it into a d.c. signal considering the difference phase.

Comparing both sensors, we notice that some potentiometers (GEFRAN, 2022) can cover a range from ± 25 to $\pm 250mm$, whereas LVDTs have displacement spans which vary from ± 12.5 to $\pm 200mm$ as in (METROLOG, 2016). The temperature effect is another important factor because potentiometers are usually more sensible than LVDTs. Furthermore, even regulation (SAE, 2018) recommends the use of LVDTs sensors, the decision between a potentiometer or an LVDT, must be analyzed, considering costs, lifecycle, and frequency operation once that the velocities performed in shock absorbers in normal usage can reach around $3m/s$, what could make a decision for a potentiometer quite reasonable.

2.7.1.2 IR Sensor

The Infrared (IR) sensors are used for measurement mainly of motion and temperature. They are divided into 2 types, passive and active IR sensors. The passive ones only receive infrared radiation, otherwise, the active ones emit and receive their own radiation. The emission mechanism works as an infrared LED and the reception mechanism is an IR photodiode.

The electromagnetic waves are spread longitudinally in a radial way and when they encounter a bulkhead they are reflected changing the direction of breeding. Whether the sensor is passive, it will be required an external source that emits IR radiation, however, the active sensors have inside of their own housing the emission and reception LEDs. The working of light-emitting diodes is based on the determined range of the wavelength. Infrared radiation can be found in the electromagnetic spectrum in the visible and microwave regions. The wavelength of the IR reading is divided into 3 bands.

The first band is near-infrared which starts from 0.75um up to 3um, the second band is the middle infrared which ranges from 3um to 6um, and finally, the third band comprises wavelengths above 6um, known as far-infrared. The resistance variation is the basic mechanism of this sensor that is caused by the infrared ray that falls on the photodiode, consequently, the output voltage is modified proportionally to the magnitude of infrared light received at the receiver. An alternative for active infrared sensor mounting can be built by the following internal circuit.

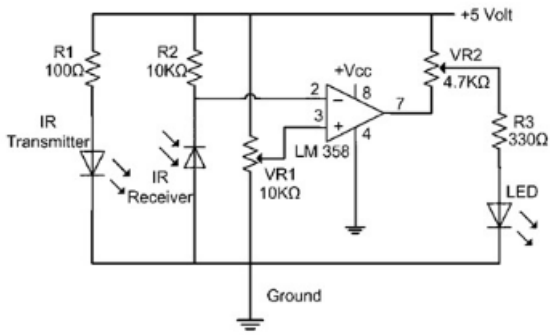

Figure 8 – Active IR sensor alternative circuit

Where the LM358 operational amplifier acts as a comparator on the circuit, receiving the voltage variation observed by the photodiode receiver in the inverting gate. Then, when no light is received, the potential of the inverting gate is higher than that of the non-inverting gate, causing the output of the comparator tending to decrease and the LED will not turn on. However, if the receiver receives IR light the inverter gate will tend to zero, making the output of the comparator rise and the LED turn on (ELPROCUS, 2022).

2.7.2 Force Measurement

A load cell is a sensor that contains strain gauges, which have a structure as illustrated in Figure 9 in its construction, being responsible for measuring force. The basis strain gauge operation is the change in the resistance due to the effect of mechanical stress (HOFFMANN, 1989). Depending on how the strain gauges are associated with each other, different types of mechanical forces can be measured.

Figure 9 – Strain Gauge adapted from (INSTRUMENTS, 1998).

The working principle is based on the relation between strain ϵ ($\frac{\Delta L}{L}$) and the fractional change in electrical resistance, defining the Gauge Factor, as k in Equation 2.16. Note that, for most metal strain gauges the Gauge Factor is usually near 2.

$$k = \frac{\Delta R/R_0}{\epsilon} \tag{2.16}$$

The measurement circuit is a Wheatstone bridge 10 with the strain gauge in one or more arms. When some force changes the strain gauge's resistance, the bridge becomes unbalanced, and this instability is proportional to the output voltage. Each application has its more useful configuration of Wheatstone bridge, for instance, there is a quarter bridge, half-bridge, or full bridge setup, and each one has its specific applications.

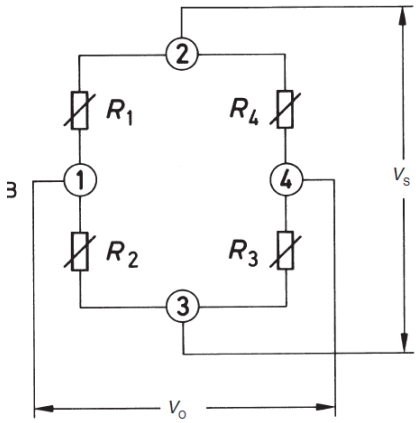

Figure 10 – Wheatstone bridge circuit (HOFFMANN, 1989).

Then, for a full bridge circuit exposed to a force, the output voltage given by the equation below is generated:

$$V_o = V_S \left(\frac{R_1 + \Delta R_1}{R_1 + \Delta R_1 + R_2 + \Delta R_2} - \frac{R_4 + \Delta R_4}{R_3 + \Delta R_3 + R_4 + \Delta R_4} \right) \tag{2.17}$$

Then, applying some simplifications according to (HOFFMANN, 1989) can be rewritten as

$$V_o = \frac{V_S}{4} \left(\frac{\Delta R_1}{R_1} - \frac{\Delta R_2}{R_2} + \frac{\Delta R_3}{R_3} - \frac{\Delta R_4}{R_4} \right) \tag{2.18}$$

Then, replacing Equation 2.16 in Equation 2.18, the output voltage becomes:

$$V_o = \frac{V_S \cdot k}{4} (\epsilon_1 - \epsilon_2 + \epsilon_3 - \epsilon_4) \tag{2.19}$$

Given this, load cells are divided into different types and classified in accordance with shape. There are beam, column, "S" and diaphragm types. Beam load cells are indicated for tension and compression, in which the force is applied on the extremes of the cell. In general, they can be used to obtain momentum forces. The column load cell is made for capture compression by vertical forces. The "S" type load cell can be used for tension and compression. The diaphragm is indicated for compression stress, its principle of work is the same, based on the deflection of the Wheatstone bridge. The lifecycle of the load cell depends on which material it is made of. For instance, if the fatigue life is 500.000 times, the weighted capacity can be loaded 500.000 times, or even more if it has been used properly, and guarantee the properties of cell (A&D, 2022).

Figure 11 – Types of load cells (HBM, 2022)

Finally, in order to choose a specified load cell to analyze its specifications, such as the operating temperature range, capacity, and sensitivity. Besides, the output voltage values have usually quite small, requiring an amplification circuit or device with high ADC resolution.

2.7.3 Speed Measurement

Regulation *ISO2631* doesn't specifies that the speed variable can be obtained either by a velocity sensor or through the first derivative given by a displacement measure as seen in Subsection 2.7.1.1. However, the last can be considered the most recommended method due to its smaller costs compared with the former. The derivative method can be implemented using a differentiator circuit shown in Figure 12 (IRWIN; NELMS, 2011).

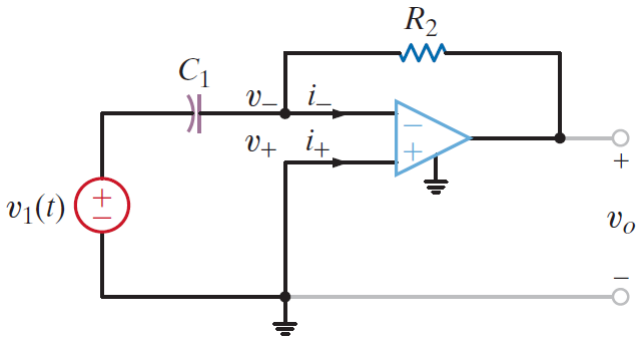

Figure 12 – Differentiatior circuit (IRWIN; NELMS, 2011)

Considering the input voltage V_1 as the output of a displacement sensor in which, V_1:

$$V_1 = k_x x \tag{2.20}$$

Where k_x represents the sensitivity of the sensor and x relative displacement. Applying the properties of an ideal op-amp, i.e. in the circuit of Figure 12 (IRWIN; NELMS, 2011), the output voltage is given by the Equation 2.20.

$$V_o = -R_2 C_1 \frac{dV_1(t)}{dt} \tag{2.21}$$

Making Equation 2.20 in Equation 2.21,

$$V_o = -R_2 C_1 k_x \frac{dx(t)}{dt} \tag{2.22}$$

That can be rewritten as below.

$$v = \frac{dx(t)}{dt} = \frac{-V_o}{R_2 C_1 k_x} \tag{2.23}$$

Notice that the values for the resistance of R_2 and the capacitance of C_1 must be chosen considering a cutoff frequency above the cycling frequency of the test, due to the behavior of the circuit as a low pass filter (DIXON, 2007).

2.7.4 Temperature Measurement

As explained in Section 2.2, the temperature variation is an essential parameter to be measured due to its effects on the shock absorber damping coefficient. Besides, it must be also controlled through a control system to maintain the testing procedures under certain temperatures, this means that many sensors can be utilised to monitor the temperature. For instance, thermocouples, Resistance Temperature Detectors (RTD), and thermistors, each of them with characteristics summarized in the Table below.

Table 2 – Comparison among Temperature Sensors (TEXAS, 2013)

Criteria	Thermocouple	RTD	Thermistor
Temperature Range	–200°C +2000°C	–200°C +650°C	-50°C +300°C
Accuracy	Medium	High	Medium
Repeatability	Fair	Excellent	Fair to good
Sensitivity	Low	Medium	Very high
Interchangeability	Good	Excellent	Poor to fair
Response	Medium to fast	Medium	Medium to fast
Overall Advantages	Self powered, simple, rugged, variety of physical forms, wide range of temperature	Most stable, most accurate, more linear than thermocouple	High output, two-wire ohms measurement
Overall Disadvantages	Non-linear, low voltage, reference required, least stable, least sensitive	Expensive, slow, current source required, small resistance change, four-wire measurement	Non-linear, limited temperature range, fragile, current source required

This table is an adaptation based on (TEXAS, 2013)

Thus, even RTDs and thermistors produce reliable measurements in terms of repeatability and show better sensitivity, the chosen sensor will be exposed to an environment with vibration due to the cycling mechanism. Then, a thermocouple transducer can be pointed as an appropriate choice because it is more rugged and has a low-cost, and still shows good interchangeability as shown in Table 2.

Thermocouples are composed of two wire leads of metals with different Seeback voltages, where the wire leads are welded together creating a temperature sensing junction (T_{TC}), that has its output voltage measured at a reference temperature (T_{CJ}) (WU, 2018). As any combination of dissimilar metals can create a thermocouple, specific letters are used to designate thermocouples by type according to the combination of metals used.

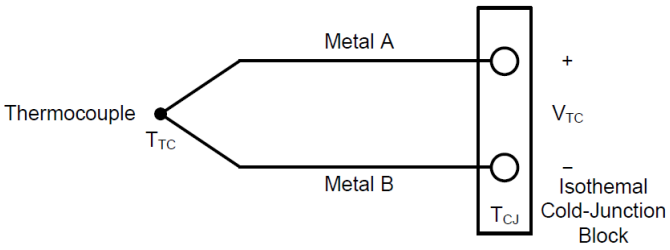

Figure 13 – Thermocouple Voltage (WU, 2018)

The most common thermocouple types are the types J, K, T, E, and S. The Figure below shows the voltage behavior due to temperature changes for each type. Lastly, Figure 14 (WU, 2018) can be also used to define the type used considering the temperature range of the demanded procedure.

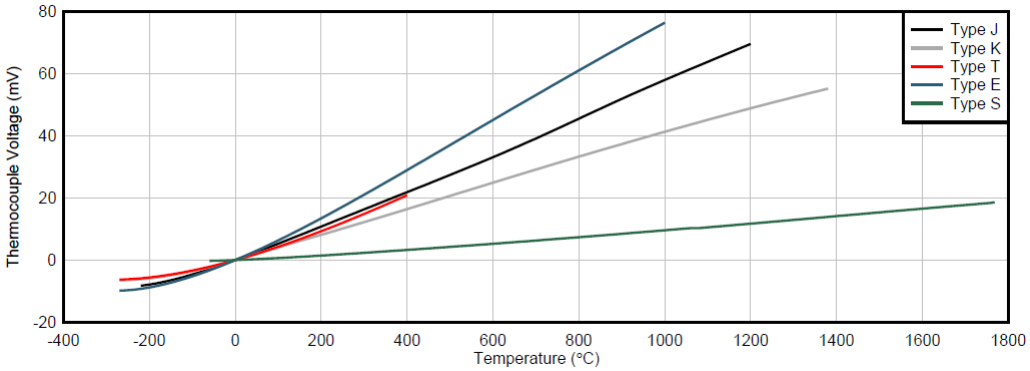

Figure 14 – Thermocouple Responses (WU, 2018).

2.7.5 Acceleration Measurement

The accelerometer is a sensor that measures a body acceleration. Indeed, acceleration is the rate of velocity change by the time. The acceleration can be measured by different ways such the derivative from body velocity, however the associated transformation errors result in large disparity of real acceleration, then it is better to use an accelerometer sensor.

There are AC-response or DC-response types of accelerometers. The AC options are charge and voltage output, both of them are piezoelectric. While DC options are capacitive and piezoresistive. Each one has its own advantages and applications (CONNECTIVITY, 2022). The accelerometers are small and there are a class of this sensors called Micro Electro Mechanical System (MEMS), that is very common used in smartphones and tablets.

Another important aspect of acceleration measuring is the behavior of payload, whether static acceleration has been measuring is properly using a DC-response, once a time it can operate down to 0 Hertz. Another situation is dynamic acceleration in which both DC and AC can be used, but a deep analysis should be made for selecting the right transductor. Above is described each accelerometer type:

- *Charge output* type is considered ones of most durable sensor, because is made based on lead zirconate titanate ceramics that offers large temperature resistance, for this is commonly used in high temperature applications. It has high impedance, then is recommended to use a coaxial cable for data transfer.
- *Voltage output* type includes a microelectronic circuit that limits the operating based on temperature. There are 2-wire and 3-wire options.
- *Capacitive* type changing the capacitance of the internal membrane in agreement with the felt acceleration by the transductor. It has a good response and requires a regulated DC voltage to work.
- *Piezoresistive* type changing the output electric signal by the internal resistance, it is not proper for the low frequencies impact, in this situation the piezoelectric has a better response, but the advantage of piezoresistive is it in high-frequency responses and impacts, such as vehicle crash test and weapon shot test.

that can be a resistor or a capacitor, it moves back and forward when suffers acceleration or deceleration, added there are stems that moves together. Between each stem there are fixed plates. The stems movement cause acceleration forces that vary the capacitance value.

In spite of exist many types of accelerometers its mechanism basis consist in measurement cell, basically the seismic mass has some stem joined in its body, when it mass suffers acceleration or deceleration the stem cause displacement between the fixed plates, then the capacitance between the fixed plates change by the mass movement, finally the capacitance value can be converted into voltage by the signal conditioning resulting in output value for acceleration, the capacitance value can be written as the equation 2.24, where A is the stem area, the ε is the relative permittivity and d is the initial distance between the plates (BENTLEY, 2005).

$$\Delta C \cong \frac{2\varepsilon A}{d^2}\Delta d \tag{2.24}$$

2.8 Pneumatic Systems

In this section, it is described the mechanisms responsible for exciting the tire and applying load over the sprung mass. In this work, it is only considered pneumatic devices, because they are safer, cheaper, cleaner, and easier to maintain compared to systems that use hydraulic components (FLOW, 2021).

2.8.1 Pneumatic Actuators

A pneumatic cylinder is an actuator that imposes force and movement through the flow of compressed air, transforming it into mechanical movement. When pneumatic actuators are used there are other components that have to be remembered, so after generating compressed air, there are air preparation, pneumatic tubes, valves, and then actuators, finally, the air will be cycling in this stages. For now, the goal is to present the cylinder and its classification. There are single and double-acting versions of pneumatic actuators.

The Figure below shows the main parts of the double-acting pneumatic cylinder. The air passing through cap-end port (A) pushing up the piston (D), extending the piston rod (F) in forward direction. When piston is moving the air has been also moved in the cylinder barrel (E). Such that this moved air goes out through the rod-end port (C). The pneumatic cylinder is reinforced by the tie rod (B) that also follows the piston shape and it is commonly made of aluminum. If the customer needs to retract the piston rod, it will be necessary input air by rod-end port and it is expected the air goes out by the cap-end port. Indeed, this mechanism is called cylinder double-acting, in which the user can control the cylinder directions.

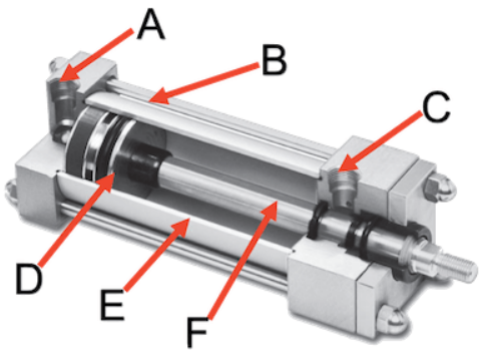

Figure 15 – Double-acting pneumatic cylinder parts (TAMESON, 2022)

While single-acting is a cylinder that is powered by only one side and its returns can be by a spring or supported weight. The pressurized line can operate extending piston rod, which is known as positive movement or operates only returning piston rod as negative movement (TAMESON, 2022).

Besides, it can be noted that there are several types of pneumatic actuators, such as:

- Round Line is a non-repairable cylinder that as known as hard-working, long-lived, and has an economical performance in terms of energy consumption;
- NFPA is a tie rod cylinder featured with a durable and repairable design. It is available in many stroke lengths and sizes;

- Position Feedback has sensors inside itself that share position like as output voltage to the external controller. Then a closed-loop controller adjusts voltage and pressure for the right position to maintain closest to the reference position;
- Diaphragm Cylinder or thruster has a small stroke and large diameter cylinder, its stroke is around one-third of the diameter and it is useful for high forces and small stroke applications. The diaphragm is responsible for the piston rod displacement instead of the piston;
- Rodless cylinders came to supply the need for an actuator where the physical space is essential, avoiding the piston rod occupied space. Their most advanced type is made of magnetic detectors at each end. This mechanism allows the displacement of the carriage rather than the piston.

It mentioned only a few actuators, but there are a lot of other cylinder types for different applications like Compact, Narrow Profile Air Tables, Twin Bore, Guided Thrusters and there are others available in (BIMBA, 2022).

The cylinder can be designed by force, pressure, and speed. Thus, by the equation below

$$P = \frac{F}{A} \tag{2.25}$$

is possible to enhance the force by growing up the section area of the piston rod by the same pressure. It is also possible tuning the forward or backward speed with a regulator valve, that controls the air flowing through the screw opening. Notice that each application will require determined values of pressure and actuating velocity. It is only possible for double-acting cylinders, for single-acting the return will depend on their spring coefficient.

2.8.2 Control Valves

Pneumatic valves are electromechanical devices used to control the direction, pressure, and flow of compressed air. In this work, a control valve will have to role to promote position and speed control of the advance and retreat of a cylinder spool to generate the road profiles. According to (WOJCIK, 2022), there are essentially three types of valves, briefly explained below.

- Switching Valve - it has only the on and off states behaving as well as an electrical switch, it allows either passing or blocking the fluid. Being more indicated for operations that demand constant cylinder speed.
- Proportional Valve - that has the characteristic of allowing the passage of compressed air proportionally to the input voltage or current DC acting in their solenoids, being

quite suitable for complex tasks that require flow and speed control with precision of the output signal.

- Servo Valve - it usually demonstrates higher precision among the other types, being applied with closed-loop systems and elaborate electronics, and is more expensive compared to other valves.

Thus, in order to avoid the elevated prices of servo control systems and the inflexibility of air flow control of switching valves, proportional control valves are commonly used as a device control of a large number of applications. For instance, through the charts provided by the manufacturer in figures 16a 16b (FESTO, 2022) the forward and backward movements alongside a displacement sensor and a controller can be used to create an accurate positioning control system.

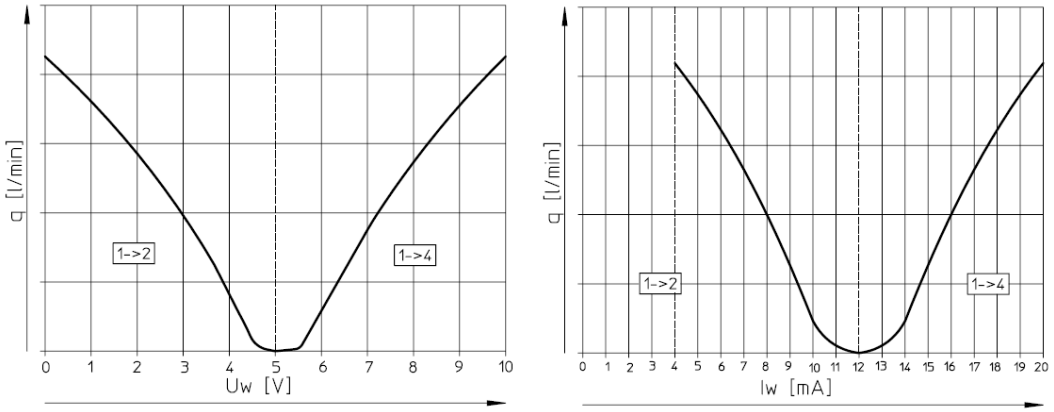

(a) Valve response curve by voltage input (b) Valve response curve by current input

Figure 16 – Proportional Directional Control Valves Response Curves (FESTO, 2022)

From that, for the valve illustrated in Figure 17, applying a signal inside the range of before the turning region the advancing occurs on the transition from 1 to 2 while port 3 exhausts, as for a ranging signal after turning region of the curve the retreating operation on the transition from 1 to 4 and makes port 5 exhausts.

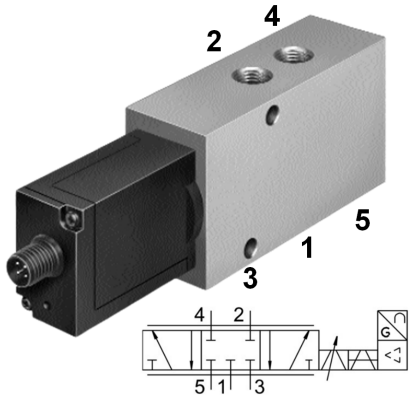

Figure 17 – Proportional Directional Control Valve (FESTO, 2022)

It is noteworthy that controlling this technology is a challenge and some variables should be taken into account. The air is a compressible fluid, so this is a non-linear system and presents difficulties in modeling, furthermore, friction, and control of force and position, are also parameters that can influence the behavior of the valve.(MENG et al., 2011)

2.9 Control Systems

A control system is defined as a set of devices capable of giving a desired response to a given process. It can be implemented in an open-loop or closed-loop. Thus, for an open-loop system, there is no feedback path, making the control action independent of the plant output. As for the closed-loop systems, there is a feedback path, which allows the control action to be dependent on the plant output signal, ensuring the system performs corrections and mitigating the errors present in the system.

2.9.1 Proportional-Integral-Derivative Controller

Controllers are mechanisms used to improve the performance o system acting directly on the error present in a closed-loop system. Among these, there is the (Proportional-Integrative-Derivative) PID controller, which is widely used in most control processes in the industry until today, (ANG; CHONG; LI, 2005) and (BRIEFS, 2014). Being composed of three terms as follows:

- Proportional (K_p): provides to the system a control action proportional to the error, ensuring a faster response, and reduction of the steady-state error. However, its value must be carefully chosen, as very high values tend to make the system unstable.
- Integral (K_i): its integrating action acts on the accumulated error, integrating the correction signal over time, being even more efficient in reducing the stationary error when compared to the action of a proportional controller. In addition, the choice of this parameter must consider that too large values tend to make its action very slow.
- Derivative (K_d): acts applying the early correction of the error, improving the transient response of the system, reducing its settling time, and increasing the stability of the system. Note that for quite sudden oscillations, the derivative action tends to cause large instantaneous increases in its derivative action.

Considering a generic closed-loop control system as the Figure 18

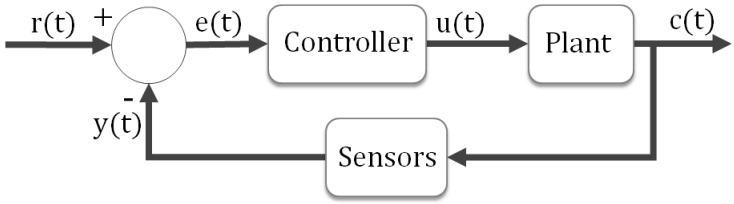

Figure 18 – Control system diagram.

Its controller function in the time-domain can be given by Equation 2.26.

$$u(t) = K_p e(t) + K_i \int_{t=0}^{t} e(t)dt + K_d \frac{de(t)}{dt} \tag{2.26}$$

in which $u(t)$ is the control action to be sent to the plant of the system, and $e(t)$ is the input error represented by the equation below.

$$e(t) = r(t) - y(t) \tag{2.27}$$

where $r(t)$ is the input reference and $y(t)$ is the system output signal.

As most applications are currently applied to microcontroller systems, in order to use a PID controller, Equation 2.27 must be used in the discrete-time form, as in Equation 2.28.

$$u(kT) = K_p e(kT) + K_i T \sum_{k=1}^{n} e(kT) + K_d \frac{e(kT) - e(kT - T)}{T} \tag{2.28}$$

with $u(kT)$ and $e(kT)$ are the control and error signals in discrete-time while T is the sampling time.

2.10 Data Acquisition Systems

Data acquisition is the process of capturing signals and characteristics from the real world and converting them into data information that will be processed by a computer (NOTES, 2022). In addition, it allows monitoring of a system's behavior and verifying if is operating appropriately as designed. Bellow, it is represented a general schematic process of a data acquisition system.

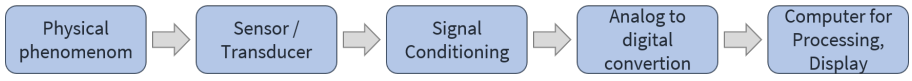

Figure 19 – Data acquisition system schematic. Adapted from (NOTES, 2022)

The advantage of data acquisition systems is that many variables readings to one computer such as temperature, force, velocity, displacement, voltage, current, pressure, angle, and others can be acquired together at elevated acquisition rates. In some standards might possibly be required primary and secondary constants, then it can be obtained by the data acquisition system by selecting a few sensors that are the basis and then it will be possible to discover the derived or secondary values from the first. For instance, speed and acceleration can be obtained from first displacement and second displacement derivatives. Notice that by doing this study of variables needed is possible to reduce costs.

It is very common to use a data acquisition board with its additional modules. These modules incorporate A/D or D/A converters, and signal conditioning circuits, and are capable of providing better synchronization data and minimizing errors.

3 Project Development

As observed in Chapter 2, the quarter-car vehicle model can be utilized in order to evaluate the suspension performance, in terms of comfort and safety, using vertical dynamics analyses as recommended in (RAJAMANI, 2006) and (GILLESPIE, 1992). Based on that, to automatize the test procedures, the variables suspension travel, suspension travel rate, vertical acceleration of chassis, vertical acceleration of wheel, the vertical load applied to the wheel, and temperature must be monitored.

3.1 Test Rig Overview

The present automation object consists of a quarter-car test rig that has undergone through development process since 2018, Figure 20. In its current stage, the rig does not allow a thorough analysis of the vertical dynamics behavior due to restrictions in the realization of vertical movements of the sprung mass. However, even with such constraints it permits testing different geometry suspensions.

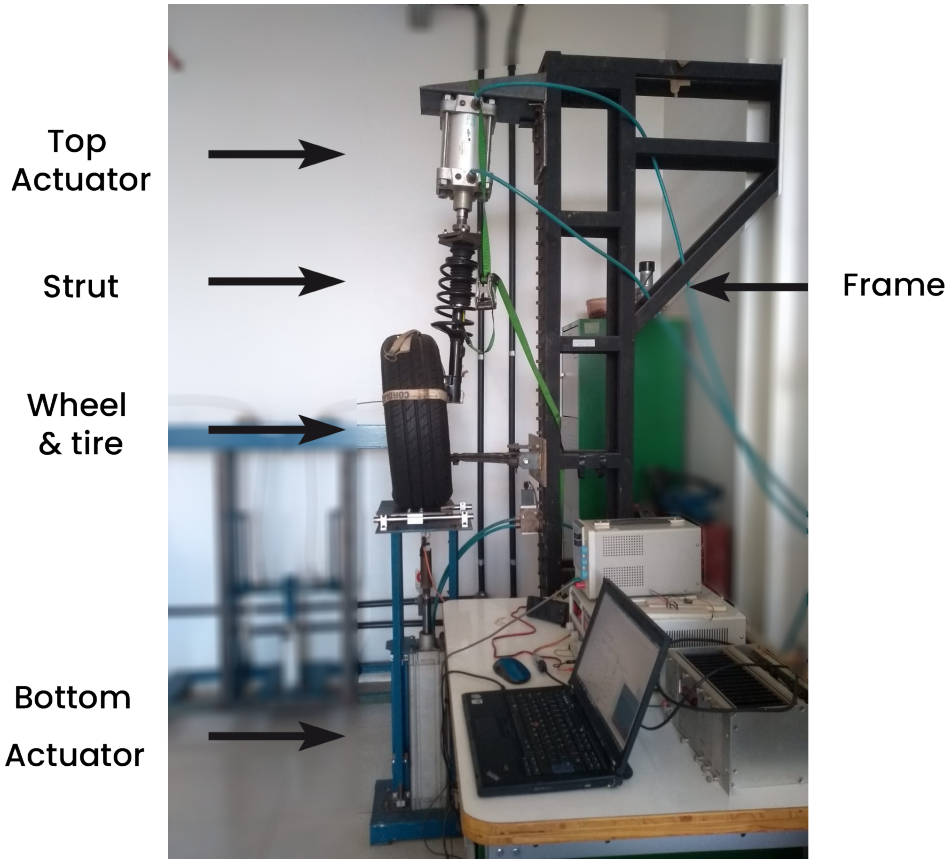

Figure 20 – Quarter-car test rig

The main components of the rig are the top and bottom actuators and their supports,

the frame, and the tested system which is represented by a quarter-car model, which is, the wheel, tire, control arms, and hub. The main components of the rig are described in the following sections.

3.1.1 Top Actuator

The top actuator DNG-160-100-PPV is attached to the top support, in order to generate the sprung mass of a quarter-car model. According to its datasheet, it can operate from 0 to 6 bar, it has a stroke of 100 mm, and its theoretical advancing and retracting force, at 6 bar, are 12064 and 11310 N.

3.1.2 Bottom Actuator

The bottom actuator is connected to the basis of the frame using a fixed on the ground structure. Its function is to generate the excitation input for cycling the quarter-car model. The used model is a DNC-125-400-PPV, that has 400 mm of stroke, operating pressure ranging from 0 to 6 bar, and also is capable of exerting an advancing and retracting load of 7363 and 6881 N.

3.1.3 Top Actuator Support

This component is attached to the superior part of the frame and it can be moved up or down to change the position of the top actuator. In addition, it is used to keep the structure stable preventing undesired movements.

3.1.4 Bottom Actuator Support

Attached to the inferior part of the frame, it is responsible for fixing the bottom actuator in a stable position. It also has an external structure that ensures that the input signal acts only in vertical directions through guiding elements.

3.1.5 Frame

It is a fixed to the ground structure with high stiffness that must remain motionless during the tests to mitigate systematic errors in analysis results and, at the same time, increases the robustness of the rig. In addition, it actuates as a support for mounting suspension, and due to its dimensions enables the rig to test several types of suspensions.

3.1.6 Embedded electronics

It covers sensing elements and how to establish communication and share data with the cDAQ, as well as comprehends the laptop interface interaction which makes it possible

(a)

(b)

for the user to view the live charts. The embedded electronics also carries the cables and connectors standards, into separated voltages and power.

3.1.7 Pneumatic system

The pneumatic system is composed by a pneumatic cylinder, an air treatment unit and tubes. The inside the room pneumatic line is controlled by a pressure gauge or a manometer. When the compressor reaches out 12 bar, the motor is turned off and then the pressure falls down. When it hits 9 bar, the compressor is turned on.

3.2 Functional Requirements

In order to define the operating conditions that the measurement system will be exposed, the following requirements were proposed:

- To measure the load applied to the tire up to 6000 N;
- To measure the displacement between the road and the tire;
- To measure the vertical road displacement;
- To measure the displacement between the chassis and the wheel center;
- To measure temperatures from -40º to 140ºC;
- To measure suspension travel rate up to 3 m/s;
- To measure chassis acceleration up to 3 m/s^2;
- The excitation frequency must be in the range of 0.5 Hz to 15 Hz;

- The working temperature of the shock absorber must be in the range of -40 to 140 ºC.

3.3 Proposed Solution

Given the elements already presented in the Test Rig as exposed in Subsection 3.1, the proposed hardware, software, and human-machine interface solution can be described as the model depicted in Figure 21.

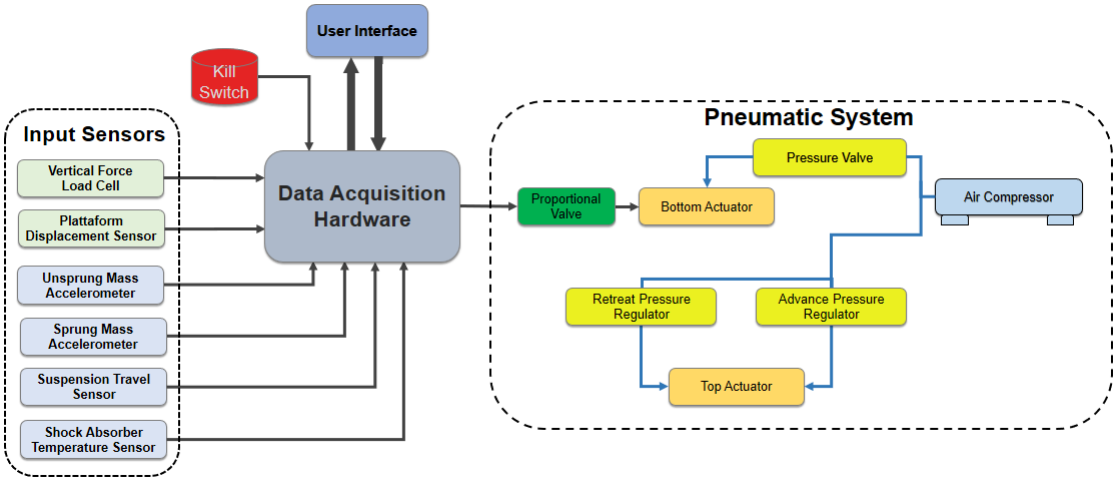

Figure 21 – Schematic Solution

From this, it can be seen that the system is composed of 4 parts, as follows.

- *Data Acquisition Hardware* - it is composed of three development boards: NI 9219, NI 9234, and NI 9264; and it is designated to acquire and process data from the input sensors and control the signals sent to the bottom actuator which integrates the pneumatic system.
- *Input Sensors* - it is a set of sensors utilized to get the data from the suspension to the Data Acquisition System.
- *User Interface* - it is used to provide an interface for the user to be capable of setting the restrictions to the tests through the configuration of the suspension system parameters, the offset height of the excitation platform as well as the amplitude, and the frequency of the input signal of the test. Besides, it is also used to display, in real time, and save the acquired data in a file.
- *Pneumatic System* - present since the previous projects, its structure was kept the same. It is responsible for actuating over the desired suspension, allowing mechanical control of the pressure applied on the sprung mass by the top actuator through a manual pressure valve. While the bottom actuator can be actuated by a directional proportional valve to generate road profiles.

Subsequently, Figure 22 illustrates the solution proposed from the schematic solution, where can be seen the components that integrate the measurement and pneumatic systems.

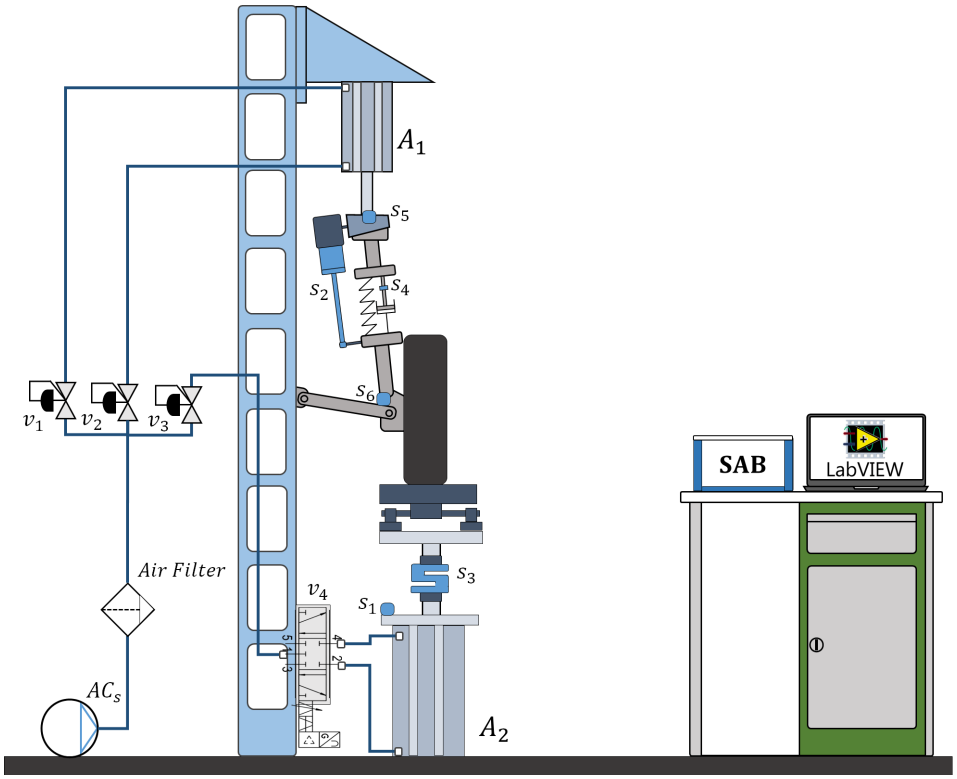

Figure 22 – Proposed Project.

where its components are grouped in Table 3 according to their function.

Table 3 – Components

Symbol	Function	Component
S_1	To measure platform displacement	Sharp Sensor
S_2	To measure suspension travel	Potentiometric Ruler
S_3	To measure the vertical force	Load Cell
S_4	To measure the shock absorber temperature	Thermocouple Type K
S_5	To measure unsprung mass acceleration	Uniaxial Accelerometer
S_6	To measure sprung mass acceleration	Uniaxial Accelerometer
A_1	To apply a load on the sprung mass	Top Pneumatic Actuator
A_2	To excitate the platform	Bottom Pneumatic Actuator
v_1	To control the advance pressure	Pressure Regulator Valve
v_2	To control the retraction pressure	Pressure Regulator Valve
v_3	To control the input pressure of valve v_4	Pressure Regulator Valve
v_4	To control the flow rate of the compressed air	Proportional Directional Control Valve
AC_S	To provide compressed air to the pneumatic system	Air compressor
SAB	to maintain the eletronic aquisition system	Electrical enclosure

3.4 Hardware Setup

3.4.1 Analog Inputs Module - NI 9219

The data acquisition board *NI*9219 has 4 channels as in Figure 23, which are channel-to-channel isolated, increasing the system robustness, and yet provide functional safety because even if a failure occurs in one channel the other will keep working without being affected (KAMATH, 2020). Another valuable characteristic of this device is that allows signal conditioning for a wide variety of measurement types, such as thermocouples, RTDs, strain gauges, and others making it a great choice for acquiring the required data from sensors installed in the suspension system, and also over the rig.

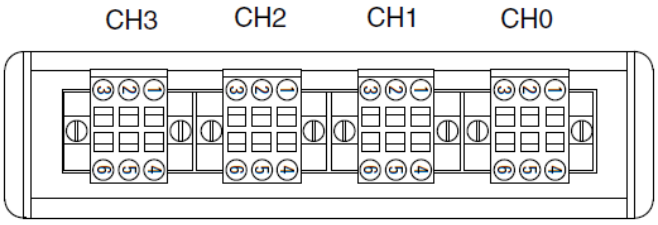

Figure 23 – NI 9219 Connector Assignments (INSTRUMENTS, 2017)

Besides, it allows to set up four types of manageable timing modes considering configured channels as one or more thermocouples. The first is high-resolution, which provides maximum noise attenuation beyond rejects the 60 Hz and 50 Hz with an acquisition rate close to 2 Hz. The second is timing modes of 50 Hz rejections which provide 50 Hz noise rejection at an acquisition rate of 7.14 Hz. The third is the 60 Hz rejection timing mode which guarantees 60 Hz noise rejection at an acquisition rate of 8.33 Hz. Last, the high-speed timing mode optimizes the sample rate and allows an acquisition rate of up to 50 Hz.

3.4.2 Acceleration Acquisition Module - NI 9234

To monitor the acceleration data of the sprung and unsprung mass, the NI 9234 dynamic data acquisition module is used, which, as illustrated in Figure 24, has four input channels. In addition, it incorporates the necessary signal conditioning to process data from sensors that use piezo-electric technology to capture vibration, pressure, or force signals, thus being widely applied in measurements of Integrated Electronics Piezo-Electric IEPE sensors. Finally, the module also includes an anti-aliasing filter that automatically adjusts itself considering the sampling rate used during the data acquisition process.

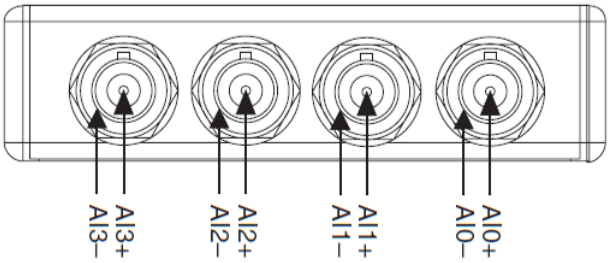

Figure 24 – NI 9234 Connector Assignments (INSTRUMENTS, 2021)

3.4.3 Analog Output Module - NI 9264

NI 9264 has 16 channels, where the AO pins are the analog outputs, while the COM pins are the common reference to isolated ground. Each channel has overvoltage and short-circuit protection which makes it quite rugged, and also capable of producing an output voltage ± 10 V with an ADC resolution of 16 bit working inside of the range of the proportional directional control valve seen in Subsection 2.8.2.

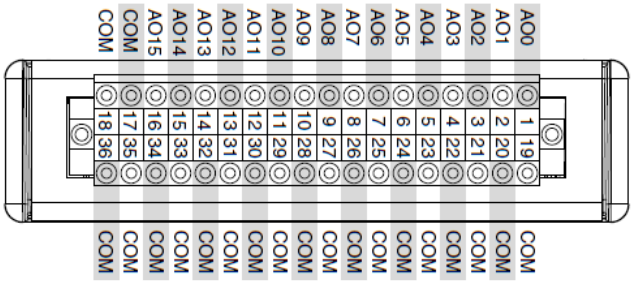

Figure 25 – NI 9264 Pinout (INSTRUMENTS, 2016)

Furthermore, this device has a writing sample rate of 25 KS/s/ch. Being capable of working in accordance with the minimum sample rate of 30 S/s required to generate the excitation frequency over the suspension system. Due to such characteristics, the development board NI 9264 was designated to control the actuators.

3.4.4 Integration Chassis - NI 9172

To integrate the three modules NI 9219, NI 9234, and NI 9264, it is applied to the project the National Instrument Compact Data Acquisition (cDAQ-9172) chassis. The utilized board has slots for 8 modules of acquisition. Besides, the $cDAQ-9172$ has four 32-bit general-purpose counters and timers, allowing the acquisition of analog signals with three independent rates. Additionally, according to its datasheet (INSTRUMENTS, 2008), the DAQ system has one AI timing engine to generate its sample clock. Thereby one analog input task is permitted to run at a time, but it can include channels from multiple analog input modules.

Figure 26 – Chassi CompactDAQ (INSTRUMENTS, 2022)

3.5 Input Channels Configuration

3.5.1 Vertical Force Acquisition Channel

As the NI-9219 has support to make measurements in Full-Bridge configuration, the force will be read by the input ports (HI and HO) differentially, and then will be sent to ADC to read the voltage between them.After that, it will be measured and monitored the vertical loads which can reach up to 7.363 N during the tests. It was selected an S-type load cell, Figure 27, with a measuring capacity of 10,000 N, an operating temperature of -10 to 60ºC, a rated output voltage of ±2 mV/V and a recommended excitation voltage from 5 to 10V.

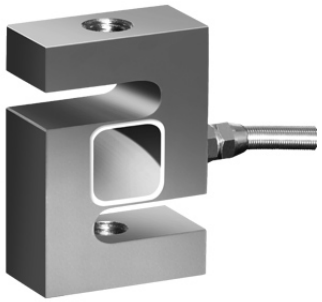

Figure 27 – S-type load cell TSA.

As load cells have usually low output voltage levels, it is necessary to use an accurate voltage source because when its Wheatstone bridge is excited with an unstable voltage source, its output voltage becomes quite compromised. Therefore to read its output signal the configuration for the full-bridge circuitry of NI-9219 was selected following the configuration in Figure 28 (INSTRUMENTS, 2017). Then, using the maximum value of 2.5V allowed by the device as an excitation source to supply the bridge, the load cell, at its full mechanical load, shows an output voltage of 5 mV. Notice that though the supply source is out of the recommended range, the NI-9219 is able to provide high resolution because the output voltage is read differentially with a resolution of 149.01nV by the 24 bits ADC.

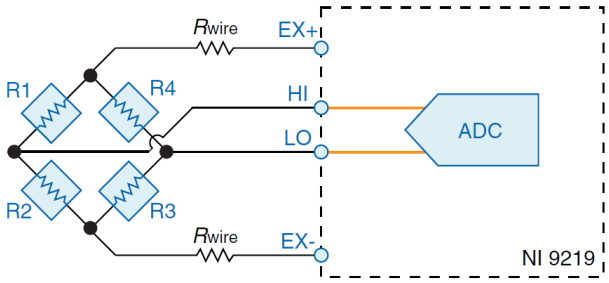

Figure 28 – Full-bridge circuitry (INSTRUMENTS, 2017).

3.5.1.1 Load Cell Calibration

With the parameters defined, it is possible to make a calibration curve. The calibration procedure consists of the force transducer compression and tension submitted by a fatigue machine. The laboratory load cell supports until 10000N in both directions. For the experiment, the transducer is excited in the range of -8000N up to 8000N. In addition, the calibration must be taken on the same VI software that will be used for the final suspension application. The National Instrument developed this feature in order to validate sensor calibrations to that VI, as well as figure out the expiration date.

The Instron 8801 was used for tension and compression of the load cell with steps of 1000 N, from 0 N up to 8000 N and 0 N up to -8000 N, as it can be seen in Figure 29a. It was adopted between 15 to 20 seconds of waiting time for collecting accurate data. In practical terms, it is difficult setting the right measurement as 1kN, 2kN, 3kN, and so forth. In summary, the reference force values measured by the load cell were approximately the expected values, see in Figure 30. From Instron Bluehill software, it is showed the applied load to the load cell, therefore this is the reference value that the load cell and VI software must show to the user.

(a) Load cell attached to Instron (b) Load cell calibrating values

Figure 29 – Load cell calibration procedure (FESTO, 2022)

This calibration procedure is essential because the VI calibration updates the output values, based on the difference of reference committed by the user and the uncalibrated values as depicted in figure 29b.

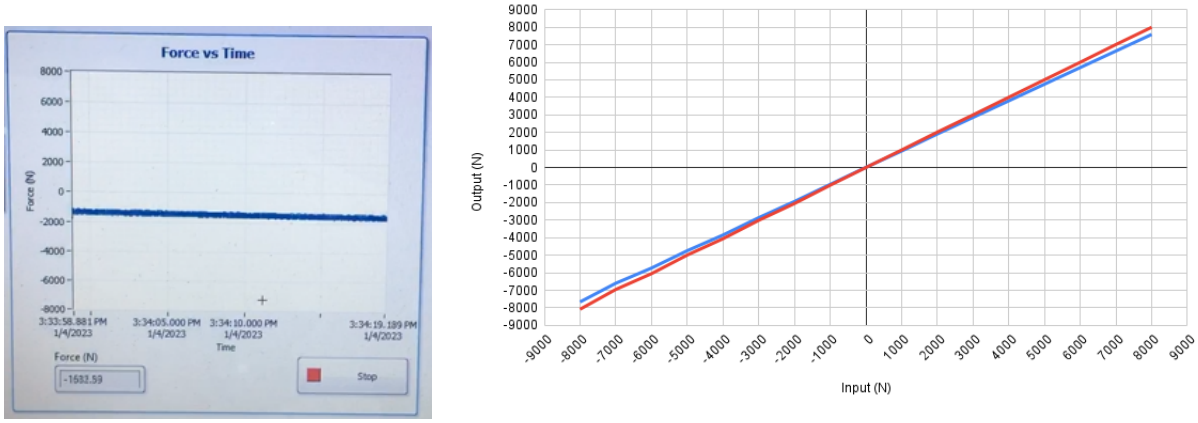

(a) Load cell curve inspection in LabVIEW.

(b) Load cell calibration curve.

Figure 30 – Load cell response curves

3.5.2 Excitation Platform Displacement Acquisition Channel

The infrared sensor utilized on the suspension test bench aims to measure the displacement of the platform connected to the piston rod of the bottom pneumatic actuator, in real-time, in order to provide it for the feedback control to use it as a reference and improve the accuracy in the process of generating the road profile, allowing to control the advance and retreat actions, and also establish the zero point to start the tests. In function of that, the distance measuring sensor selected is the model GP2Y0A21YK0F, as in Figure 31, with a measuring range from 10 to 80 cm with analog output, with a response for the first reading of 38.3 ms±9.6 ms and following readings 5 ms.

Figure 31 – Infrared Distance Sensor

After that, as this sensor is a passive type, it is powered with a DC source of 5 V. Its out voltage is directly read through the NI 9219 module ADC channel, as illustrated in Figure 32, in which the pin 1 is the input supply, pin 2 is the ground and pin 3 is the output voltage.

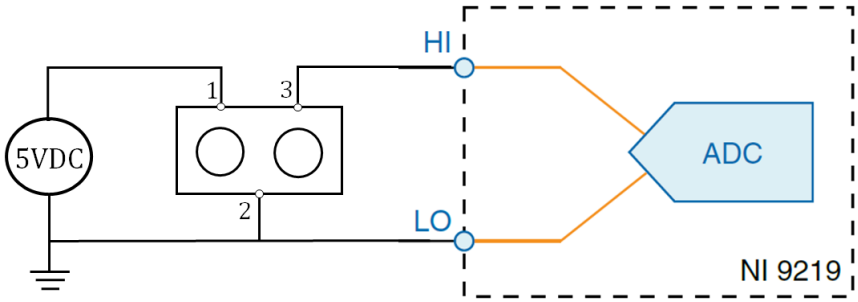

Figure 32 – Infrared Distance Sensor Connection

3.5.2.1 Calibration of the Excitation Platform Displacement Sensor

In order to define the region of operation of this measurement system the response curve must be obtained and compared with the reference curve given by the datasheet of this sensor. From this, to calibrate the infrared sensor, it was carried out an experiment as shown in Figure 33, where a ruler with a minor reading division of 0.5mm was positioned below the infrared sensor.

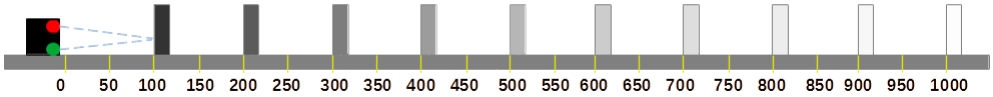

Figure 33 – IR sensor calibration procedure

Next, with the sensor positioned and fixed at a zero position, while a moving bulkhead is positioned in front of the sensor on the 0 mm position and then, the measurements were taken up to 1000 mm with 50 mm steps, and the output voltage was collected. These are the out of recommended range output values which will be collected to get precise points of linearity responses. Last, measurements were also taken in a decreasing way, from 1000mm to 0m, in order to get the sensor hysteresis curve. For each measurement taken was established 1-minute waiting time, even though the manufacturer recommends that the waiting time for the worst case the stable reading is can be taken after 43.3 $\pm$ 9.6 ms.

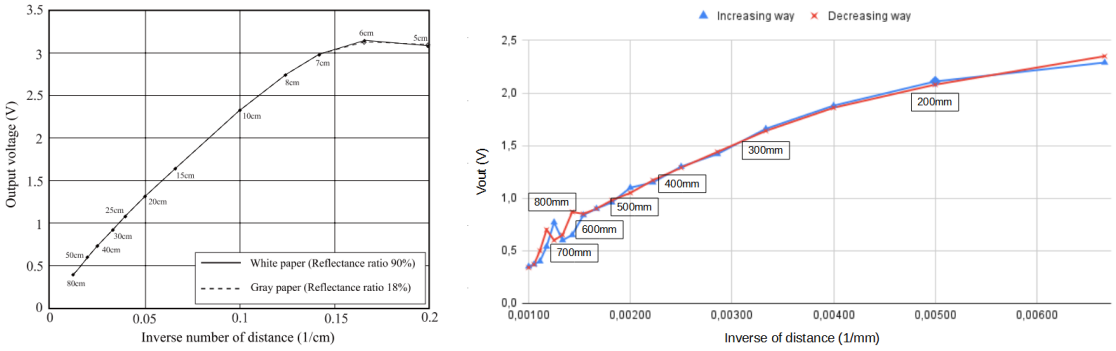

(a) IR sensor datasheet curve

(b) IR sensor experimental curve

Figure 34 – IR Sensor Curves

Finally, comparing the expected curve of Figure 34a and the response curve obtained with the experiment of Figure 34b, note the similarity between the response behavior and it is reasonable to choose the best range of work as 250 up to 650mm vertical displacement. With the measurements was also possible to verify that near 2 extreme nearest and farthest displacement output values had some errors.

3.5.3 Suspension Travel Acquisition Channel

To monitor the suspension travel, it is applied a linear potentiometer with a life of 100 $\times 10^6$ cycles. Besides that, the available electrical linear travel of 375 mm of the selected sensor, allows its installation in different suspension geometries of passenger vehicles and light trucks, whose shock absorbers show strokes below 300 mm. Another relevant parameter is its maximum working speed of 10 m/s because, through the first derivative of the displacement, we can obtain the suspension travel rate that can reach up to values of 3 m/s.

Figure 35 – Potentiometric Ruler

Then to measure the shock absorber displacement, the sensor is powered with an external voltage source of 24 V. Besides, as illustrated in Figure 36 the voltage is directly read by the ADC the NI 9219 with a configured resolution of 1.43 uV, where pin 1 is connected to the ground, pin 2 is the output voltage, and pin 3 is attached to the supply source.

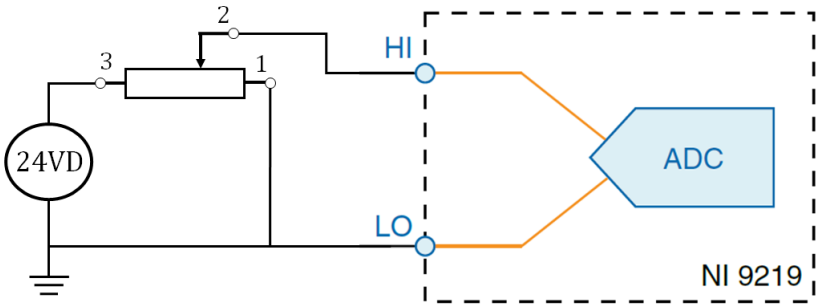

Figure 36 – Potentiometric ruler connection schema

3.5.3.1 Potentiometric Ruler Calibration

The procedure for checking the response curve of the potentiometric ruler is made outside the suspension test bench, isolated from the complete system as shown in Figure 37. In essence, the measurement output values are collected considering the gradual movement forwarding of the sensor rod. The calibration of the potentiometric ruler was based on a 1 m-long metallic ruler with a smaller scale division of 0.5 mm. For this procedure, the reference is the top of the rod ends and not it's center. Because even placing a center mark to improve the vertical visualization of the real data, there would be the possibility of moving the rod ends.

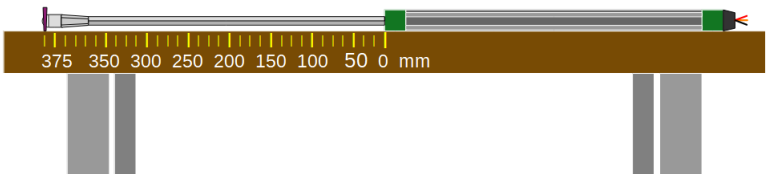

Figure 37 – Potentiometric ruler test assembly

Then, the experiment was divided into two parts, where the first part consists of collecting the output voltage values in an opening way and the second one consisted of

carrying out the same process but in the closing way, which is returning to the zero position. The measurements were made from 0 up to 380mm divided into 10 steps, which yields on 38mm increment for each step. Thus, with the acquired measurements it was plotted the response curves of Figure 38 as well as the linear equations that relate the output voltage with the displacement of the rod in both ways.

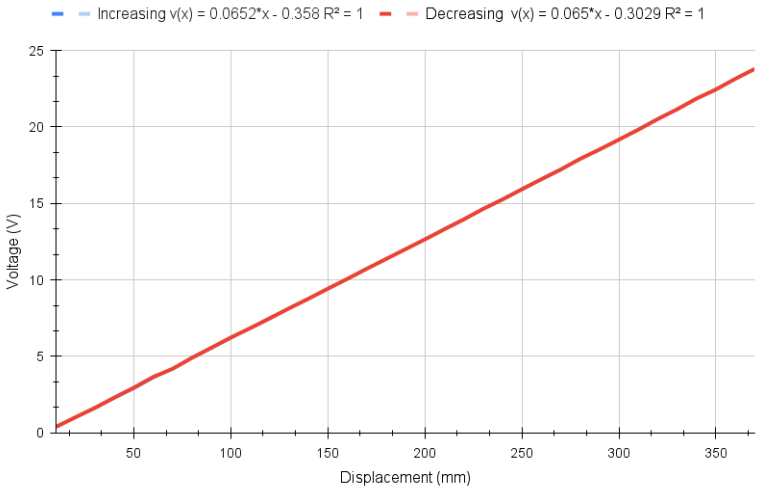

Figure 38 – Potentiometric Ruler Response Curves

Based on the potentiometric ruler curve collection procedure, it is verified that the hysteresis value is 0.088 V, but that can be neglected since with the graph of Figure 39 it was verified that the values of the coefficients obtained through the straight line of its experimental are very close as verified from the obtained equations. In addition, the offset error present in the curve is verified compared to the theoretical curve, being characterized as a systematic error, but still, it is qualified as a suitable transducer for measuring small variations in the damper displacement.

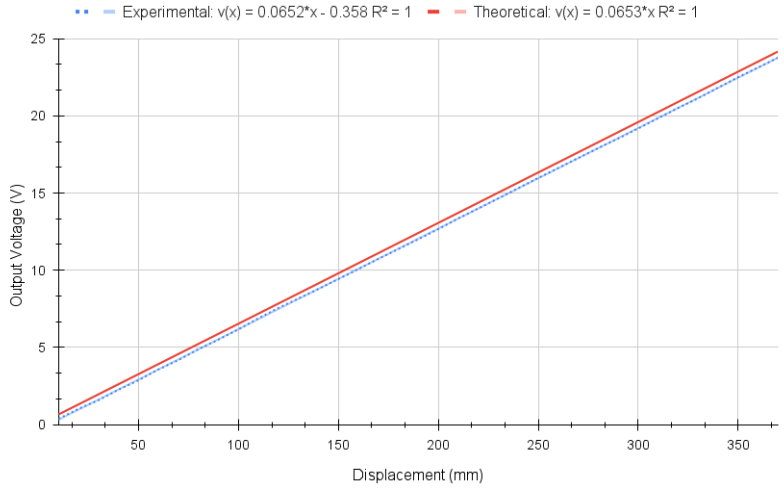

Figure 39 – Experimental Curve vs Expected Curve.

3.5.4 Temperature Acquisition Channel

NI 9219 also provides support for thermocouples, with every channel having a built-in thermistor for cold-junction compensation (CJC). That way, it was used the recommended configuration in Figure 40 to read its output voltage with the ADC with a CJC configured to read in the ±125 mV range for thermocouples of type K, and finally converted into temperature in Celsius degrees.

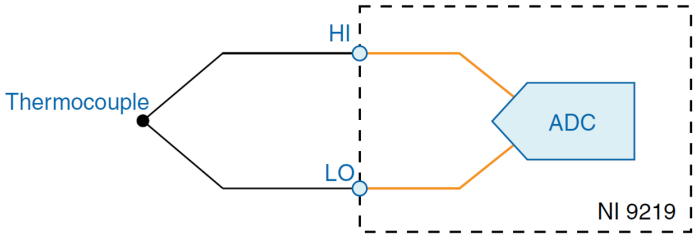

Figure 40 – Thermocouple Circuitry (INSTRUMENTS, 2017)

Last, to guarantee the adequate work of the sensor, a properly female thermocouple K-type connector and wire were utilized, and the usage of extensions and other connectors was avoided to minimize the heat transfer between the wire and the terminal junction.

3.6 Control Actuation Channel

The 5/3 pneumatic valve used in the experiment is the FESTO MPYE-5-1/4-010-B as illustrated in Figure 41, which accepts 17 VDC to 30 VDC power supply range, using an input signal from 0 V to 10 V or 4-20 mA, to control the output flow rate. Besides, it tolerates maximum pressure of 10 bar and has a frequency limit of 80 Hz.

Figure 41 – Directional Proportional Control Valve

The connection to the NI 9264 module is given in Figure 42, where pin 1 is connected to 24 V DC supply voltage, pin 2 to GND, pin 3 UW/IW, the setpoint input voltage used to control the flow rate, and last 4 that is connected to GND.

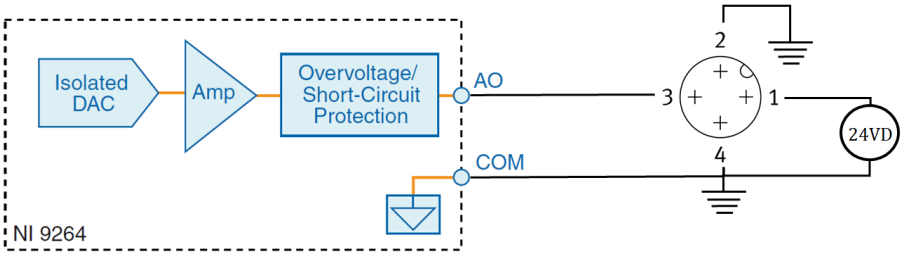

Figure 42 – Valve Connections

3.7 Electrical System

The purpose of the electrical system is to provide external connections in order to set the data acquisition system a plug-and-play characteristic and, at the same time, to organize the internal setup connections that were defined in Sections 3.4, 3.5, and 3.6. Given this, the electrical system of the box is represented through a diagram in Figure 43. The system has a general on-off switch, that when turned on allows the internal line filter to supply the DC power sources of 5 V, 24 V, and the 12 V Data Acquisition Chassis source. Additionally, it can be used as a safety element because, once it is deactivated, it ends every process which were occurring at the moment. Shutting down all the operations works regardless of software programming.

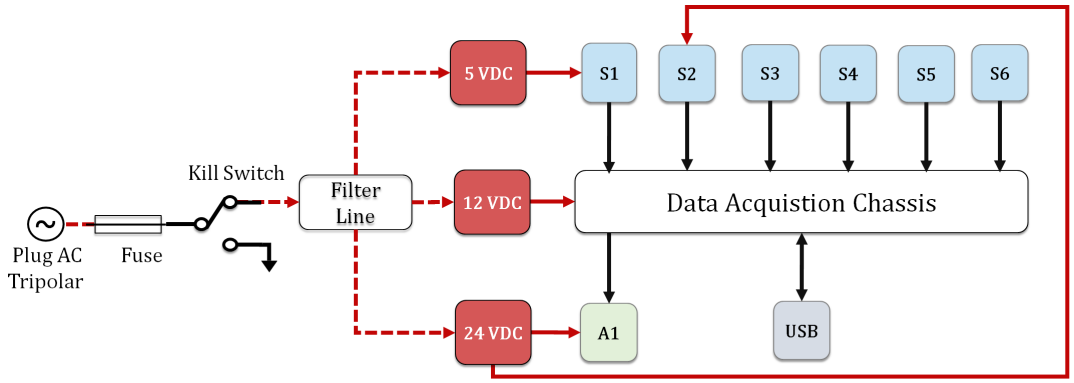

Figure 43 – Electrical Schematics.

In Figure 43, each sensor is represented by the initial letter S, and the actuator is represented by the initial letter A, which are represented in Table 4, as well as the other used connectors.

Table 4 – Connectors Applied to the Project

Device	Connector	Connects to
S1	3 Pin Female Mike	Sharp Sensor
S2	4 Pin Female Mike	Potentiometric Ruler
S3	DB9 Female	Load Cell
S4	No connector	Thermocouple Type K
S5	Coaxial Female	Sprung Mass Accelerometer
S6	Coaxial Female	Unsprung Mass Accelerometer
A1	5 Pin Female Mike	Directional Proportional Valve
USB	Female USB type-B	Computer

3.7.1 Protection Circuit

Though the cDAQ has its own protection circuitry, the sharp sensor, potentiometric ruler, and proportional valve, use external power sources that are directly connected to the power grid. Based on that, to improve the operation safeness of these sensors and reduce the risks of damage to the electronic system as a whole, it was added a line filter class III SPD that diverts the currents to the ground during the occurrence of electrical surges avoiding oscillations that may come from the power grid due to electrical discharges, and the presence of high-power machines. Besides that, it contains a micro master switch in case of overcurrent trips and turns the system off.

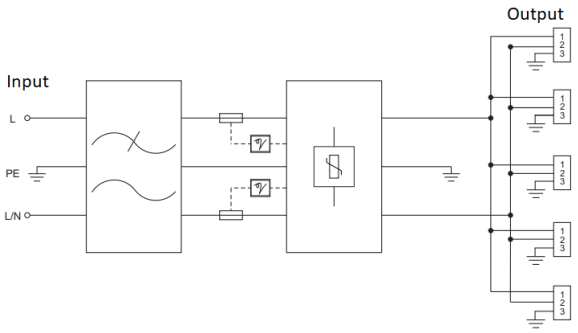

Figure 44 – Line Filter (COMÉRCIO S.A, 2021)

3.8 Electrical Enclosure

The whole set of hardware is composed of sensors and an actuator, which are diverse signals getting in and out from the data acquisition board. It was proposed an electrical enclosure that guarantees a pattern for testing and hardware settings, protects the wire connections from environmental factors, and avoids critical damage due to connection errors.

Thus, it was designed an electrical box that encapsulates the cDAQ chassis, the signals from sensors, the output signals of the directional proportional valve, and also the power sources of the system. Its rear wall holds the actuator and the sensor connectors, the ac power plug, the fuse protection, and the ON/OFF button, as depicted in Figure 45.

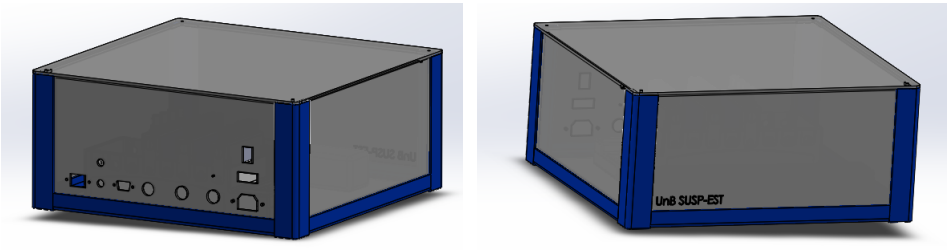

(a) (b)

Figure 45 – Backside and frontside of the SAB.

It was researched about which material would be better for the box functionality purpose, so wood and ABS 3D printing were analyzed. It was expected a well-constructed lightweight box. As a result, the final solution was 3D printing combined with HPIS .

The plastic leaf laser cutter allows to manufacture large geometries and cuts the connectors outline precisely. The vertical and horizontal columns were built by 3D printing. The fitting between these two parts is made by contact.

4 Software Development

4.1 Logic and Data Manipulation

The user interface will be developed in software LabView. The signals will be obtained from sensor entries then its going to be manipulated in LabView VI functions in order to fit a better presentation format in graphs and representative numbers, in the end classify the suspension parameters to final user.

Firstly, it is necessary to ensure the software and hardware connection, it is available by cDAQ USB port plus LabView software and NI-DAQmx Driver. Writing code by VI programs is the way creating routines and functions for conversions, using counters, controling the actuators velocity output and if it needs extend or retract. The amplitude and frequency needs to be stored in variables and arrays for after to be used in equations such road profile, for instance. In summary, all equations and thresholds will be implemented in this data processing layer.

4.2 Data Presentation

The data presentation deals with communication between humans and machines, one way is receiving some parameters from user in respect to shock absorber stroke, damping coefficient and others characteristics that be paramount significance for testing bench, as well as receiving data from sensors and generating vertical acceleration and vertical displacement graphs. Indeed, the main result is to determine road holding, suspension travel and finally, conclude about ride comfort and safety. To program in LabView is an advantage, firstly because is a visual programming language. Secondly, it is possible to handle with real-time applications. Furthermore, the LabView environment is simple to code, it is divided into Front Panel and Block Diagram. The former is what user seeing and the latter is the space for coding.

The current LabVIEW code was quite complex to understand. Then, the control approach was taken to overcome whichever difficulty. As depicted in figure 46, the code begins with the desired signal, where the user has to input the wave parameters as frequency, amplitude, offset, and phase. The second part is the control treatment of data in the distance platform control and controller block. After there is a security mechanism, in order to limit the saturated signal, and then the signal is sent to the pneumatic valve. The feedback starts with the sensor measurements, especially the infrared sensor, which controls the platform height.

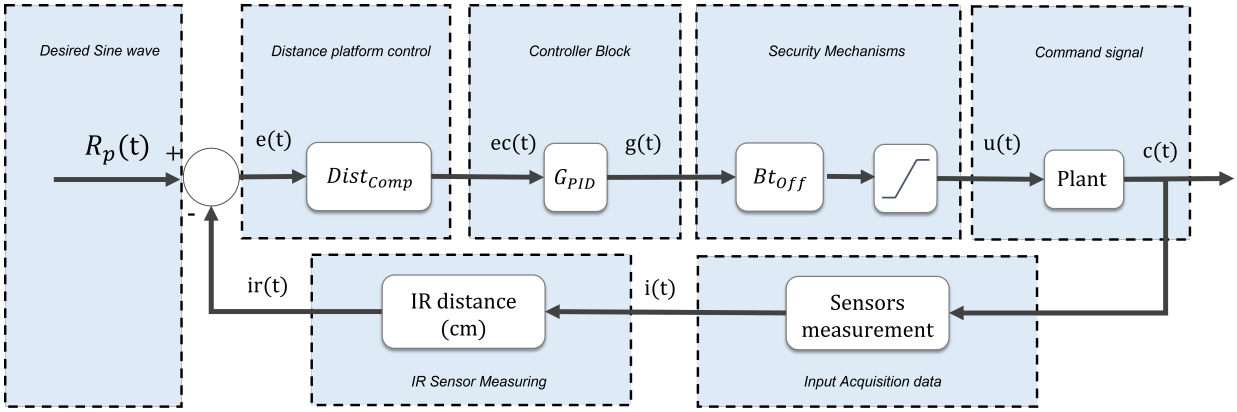

Figure 46 – Control loop approach

4.2.1 Labview code

The suspension rig code has been implemented and improved by students, so in this version it was not implemented from scratch, indeed some improvements were made in order to facilitate the comprehension of future students and for reasons of source code maintainability, as well. The real-time writing happens internally to a continuous repetition loop in which the device must acquire and process the data, make decisions based on a predefined control and then send it to the hardware with an updated signal. This mechanism establishes the experimental test. For a correct test, it is necessary to know the geometry of the suspension, for instance the shock absorber stroke and which offset distance will be adopted.

On the front panel, the user finds some blank spaces for experiment configuration, in case of this it is required to proceeds to testing. However, the block diagram screen contains the blocks with the logic. The operating principle of each block will be discussed below. Note that the used Labview version, there is no zoom feature, with that the blocks are distributed horizontally.

The first step was thought to inform the progress of the execution of the experiment, then a timer for the end of the test is introduced at the beginning of the code and on each loop the current time is subtracted, note that from this it is possible to obtain the ΔT of the loop, and when dividing by the acquisition frequency, the number of periods remaining for the end of the execution is obtained. In addition, the remaining time of execution is transformed for better visualization by the user. The arrangement of execution blocks will be treated on next section.

4.2.2 Main Blocks

The main blocks are depicted in figures 47, 48, 49 and 50. Inside of each block there is logical and other connections. It is intended to reduce the complexity of coding, separating on different VI's.

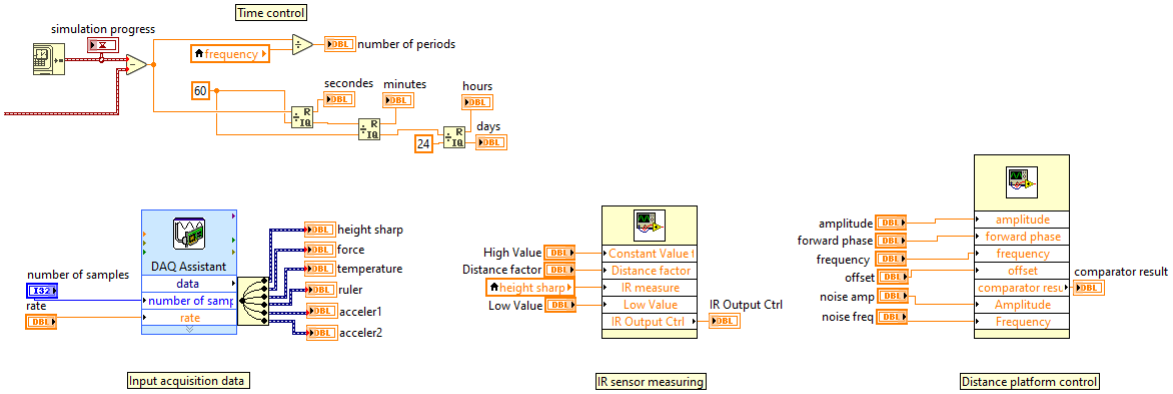

Figure 47 – Acquisition and signal analysis blocks

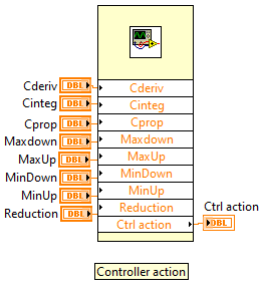

Figure 48 – Controller block

Figure 49 – Security mechanisms

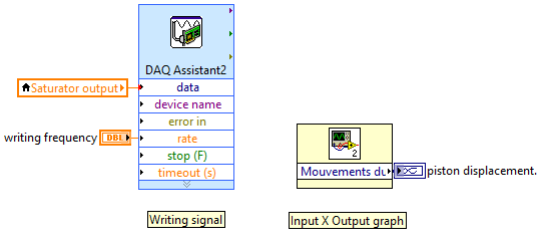

Figure 50 – Output signal

- **Input acquisition data**: In the figure 47 it is possible to see that the user might choose the reading frequency and number of samples that it is desired to acquire, finally saves it in the local variables to be used later;
- **IR sensor Measuring**: It receives the maximum and minimum advance limits data, called High and low value, respectively. Beyond that the distance factor is a sensor calibration constant to convert the measured value into the real measurement. Commonly, 60 is used as a distance factor, but it was left at the disposal of the user, for the case in which he wanted to refine the IR sensor measuring, since changing the source or even its lifetime and exposure to dust could influence the measurement taken. The IR signal is then sent to the distance control;
- **Distance platform control**: this block works as an error detector. The reference signal in the figure 47, is composed of a sine wave, due to this, this block receives as input amplitude, frequency, offset and phase advance, a second sine wave can be configured as noise in which it is possible to configure amplitude and frequency. The IR signal is inside of the distance control block where it is used table height feedback. This is the reason why the output is called comparator result;
- **Controller action**: The controller used to control the height or position of the pneumatic piston is done by PID controller, see figure 48. This controller receives proportional, integral and derivative gains. In addition, limits are established for the proportional valve '*maxdown*' and '*mindown*', which symbolize the minimum and maximum limits for piston retracting. While the variables '*maxup*' and '*minup*' symbolize the piston advance limits. With these settings, the user can establish more aggressive or smoother responses from the actuator. The 'reduction' variable acts as a response smoother when changing the direction of the piston. In practice, the piston will spend more or less time in the dead zone, a greater reduction symbolizes a greater dead zone effect, while a smaller reduction represents a lesser dead zone effect. The controller output is then passed to the subsequent block;
- **Turn off software button**: it is a trigger available to the user to take the piston to the 0 or retracted position. It is the first available security mechanism and can be seen in figure 49. The second security element is seen below.
- **Signal saturation**: it is the last block before sending the signal to the hardware, responsible for controlling the saturation of the signal. Whether the control signal is greater than 10V, then the signal sending will be 9V. On the other hand, if the signal is less than 0, the control signal will be 1V. The 9V signal will correspond to a higher speed returns and the 1V signal will correspond to the higher speed advance.
- **Writing signal**: this is where the signal tuned in the previous blocks is sent to hardware, in actually. Finally, parallel to this signal there is the 'input X output graph' block,

responsible for exhibits the input signals, the signal sent to the valve and the height of the platform in a graph. this block can be seen in figure 50;

After testing the previous version, the open-loop version of the code was developed. there was necessary to add a buffer to acquire data continuously, save and make possible future data processing. In addition, the end of the test LED indicator was built in. Another relevant feature was the possibility to change the graph window, so the user might alternate between input or output data, real-time FFT of the data, and keep up with the moving average chart. The results of the code improvement will be treated in advance in section 5.

5 Results

The whole suspension test rig is accomplished by instrumentation and actuation fronts of work as could be seen throughout the research. Due to this reason, a discussion around the selection and calibration of sensors, and the excitation mechanism used for a quarter-car test bench is presented in this chapter.

5.1 Instrumental and Robustness Analysis

After defining the functional requirements in Section 3.2, the sensors of vertical force, platform displacement, and suspension travel were calibrated except for the thermocouple and the accelerometer. As a result, they showed some restrictions. For instance, the load cell allows monitoring loads in the required range of vertical loads, besides the results demonstrated quite accurately, with a maximum error of 2.5%. As for the platform displacement sensor, its working experimental range does not allow measurements below 30.00 cm, because the errors in this region tend to increase reaching values of error superior to 4.00 %, but still ensures measurements between 30.00 and 60.00 cm and percentual error inferior to 3.00%. Finally, it was verified the potentiometric ruler, has an operating range between 30.00 mm and 370 mm, guaranteeing a useful stroke of 340 mm, with a percentual error of inferior to 2.5%, notice that values measurements below 30.00 mm were not considered due to elevated percentual errors in this region. The table below summarizes the calibration results.

Table 5 – Thresholds of the sensors

Sensor	Calibrated on	Min. Value	Max. Value	(%) Max. Error
Force	Instron + LabVIEW	-8000N	+8000N	2.65
Infrared	Manually with ruler	30 cm	60 cm	2.60
Pot. Ruler	Manually with ruler	30mm	370mm	2.2

Additionally, it was noted less deviation in output IR signal after the addition of a dedicated IR voltage source, and therefore a more stable response on the displacement of platform measurement. As a result, after the improvements in instrumentation, the suspension test rig presents more stable output values.

Beyond the exclusive sensor sources, it was included 2 SPDs, which work as electronic devices for protection for cDAQ, and 5 and 24 V voltage sources. The SPD is built for deactivation before damaging another more important part of a system. For instance, the first one of them was to include a protection fuse in the entrance of the SAB, in order

to break the filament and cause less damage to the rest of the entire system. The second artifice was the inclusion of a filter line which contains an internal protection circuit, that deactivates the power supply in case of surge currents. In the worst scenarios, the filter has an internal fuse after an energy key, also for protection against over-current. Thus, whether the first device fails to protect some over-current, the second device is available to protect the DAQ system.

5.2 Excitation Platform Operating Frequency

To generate the road profile was first applied the previous software, which uses a closed-loop implementation to control the displacement of the excitation platform and contains a PID controller that allows customization in order to improve the system response. Some experiments were executed, in which PID gains and the input signal wave amplitude, frequency, and offset were modified. However, even though the bottom actuator started following the command signal according to its reference, the output response did not follow it in a permanent regime.

In order to overcome the problems with the previous displacement excitation control a software in an open loop mode was developed. Where the initial height of the platform is manually chosen, the next step is to set up the wave frequency, amplitude, and offset, and finally, the final time in seconds for the test.

Concerning the discussion above, it was tried to validate the test rig response, and for that, decimal values from 0.5 Hz up to 1 Hz frequencies and amplitude of 2 V were applied as input, was noted that the cDAQ command signal did not reproduce a sinusoidal output displacement. In Figures 51 and 52, it is possible to compare 2 sinusoidal signals that were tested, from which it was verified that the acquisition system was not able to generate fractional frequency values, allowing only integer values frequencies. Notice that, all fractional frequencies responses tested are available in annex A.

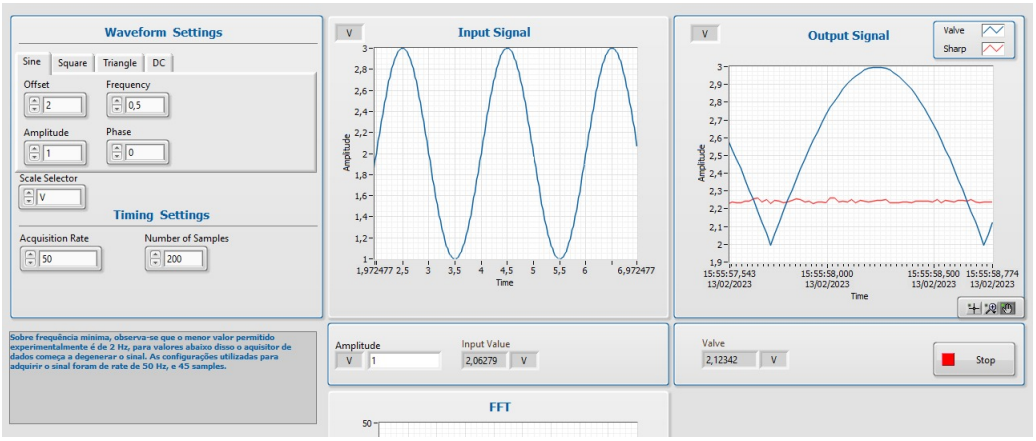

Figure 51 – 0.5Hz sine wave

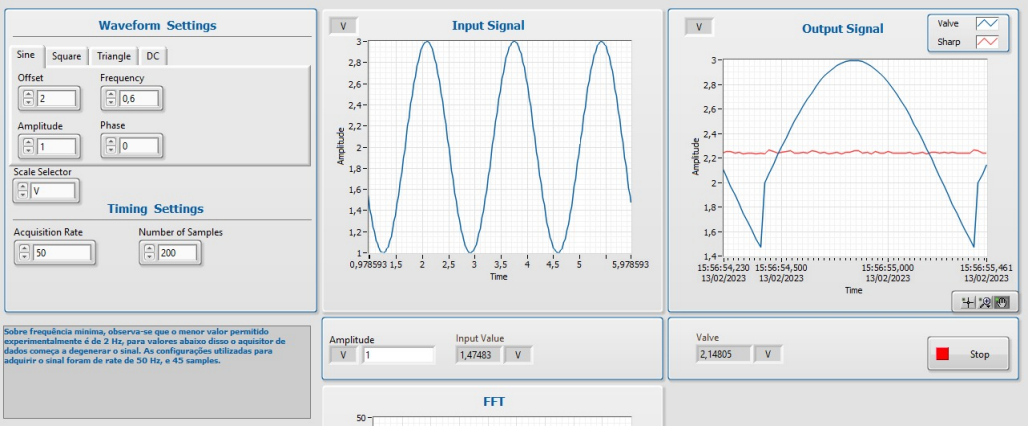

Figure 52 – 0.6Hz sine wave

With the minimum step of 1 Hz for frequency input accepted by the test rig taking into account the vibration and pneumatic actuator limit, it was defined as a maximum input frequency with a value of 10 Hz.

Next, the excitation platform behavior was analysed in the range of 1 to 10 Hz and was realized that for frequency values close to 1 Hz the IR sensor response showed the best behavior. Thus, Figure 66, the green curve at the output signal chart, that the IR sensor generates a smooth curve. In contrast, Figure 70, following the green curve at the output signal chart, that is the 7 Hz sinusoidal wave with a difficult signal.

At the stop the frequency value of 10Hz as depicted in Figure 72, the IR sensor was not able to read the excitation platform displacement properly. It was noticed that at high frequencies such as 8 to 10Hz the amplitude signal presents a tiny deviation. Then, at the faster operating condition, the loss of data was observed, and because of this, the output signal tends to be unrecognizable at high frequencies. Hence, it would be recommended to use an IR sensor with a smaller response time or change to another sensor such as the LVDT or potentiometric ruler.

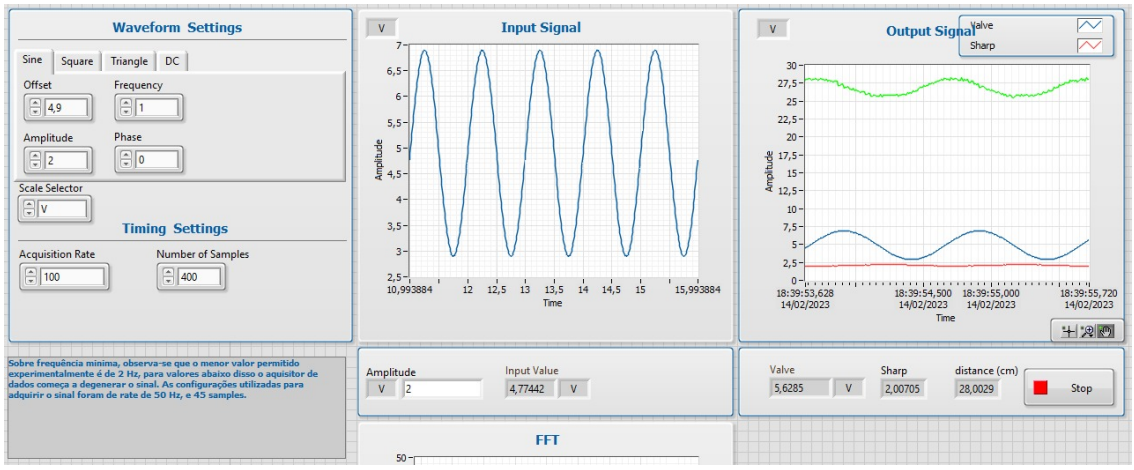

Figure 53 – Input signal of 1Hz and 400 samples

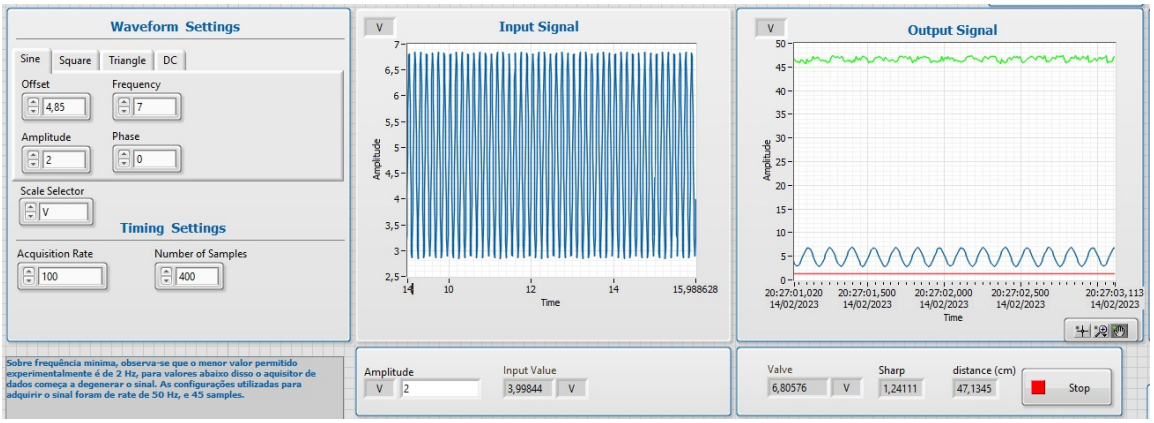

Figure 54 – Input signal of 7Hz and 400 samples

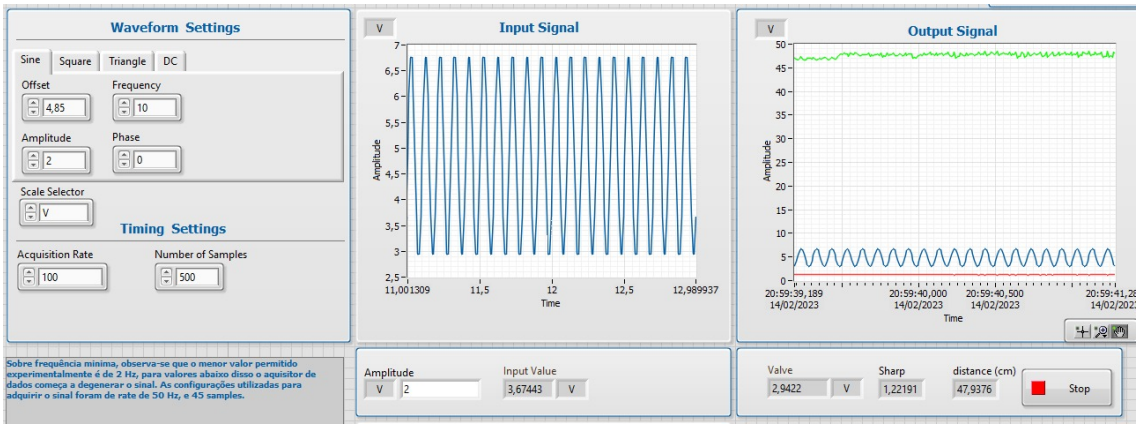

Figure 55 – Input signal of 10Hz and 400 samples

The entire range of frequency graphs such as 1, 2, 4, 5, 7, 8, and 10 Hz are available in the annex B section.

Furthermore, it was desired to map the behavior of the test bench, then vary the frequencies, and save its data in a buffer, it was possible to create magnitude and phase bode plots, as showed in 56a and 56b, respectively. The response of phase at the Bode plot begins in advance at 1 Hz and the change in phase was observed. Then, as long as the frequency get higher the phase was getting late. For instance, the lag phase was observed at higher frequencies, from 4 to 7 Hz. Also, in the magnitude plot, figure 56a, there is a rebound of a signal between 2 and 3 Hz, which indicates one more pole appearing. The behavior of the system reminds a third-order system or greater than second-order systems, as expected from a quarter-car test bench. Therefore, it can not be confirmed because there is a hardware limitation in using fractional frequencies, then the range of values is too restricted, and there are missing data between integer values of frequency. More details about system control are not in the scope of this work.

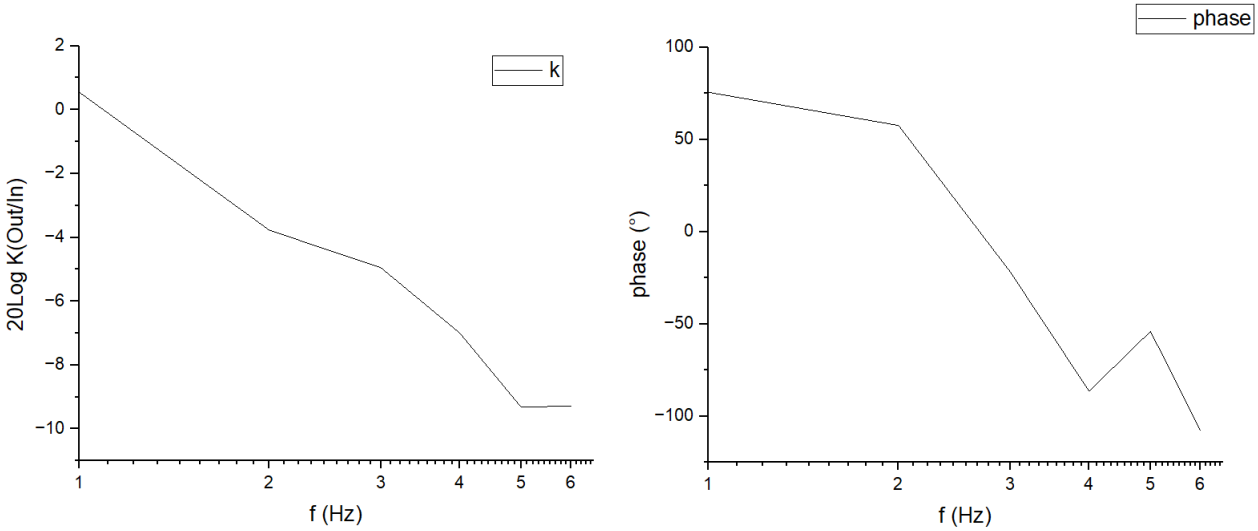

(a) Magnitude plot (b) Phase plot

Figure 56 – Bode plots

5.3 Usability

Finally, the previous test bench version is compared to the modified one, then the without and with encapsulation proposals are shown below in the figures, 57 and 58. The physical upgrades are to avoid incorrect connections and to provide only one wire to turn on the system. After the electrical enclosure was developed, running tests became a plug-and-play activity. That afforded to focus on the software development, exploration of sinusoidal track profiles, and the validation of the responses of the sensors.

(a) (b)

Figure 57 – Suspension test rig before changes

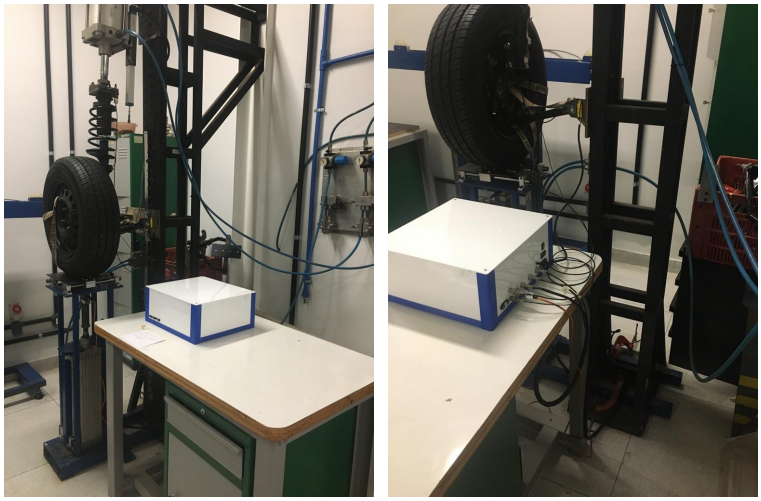

(a) (b)

Figure 58 – Suspension test rig after changes

The final software solution is the user interface. In figure 59 the green indicators mean the order for setting up the experiment. In this stage the user can select the input wave signal, it can be sine, square, triangle, and constant (DC). Next, the wave parameters can be set as frequency, offset, amplitude and phase. After that, the user can choose the scale of the data. Finally, the user might configure the timing settings as acquisition rate, and the number of samples of the data.

The second part of the interface is shown as yellow blocks that represent the test information, such as a graph, current execution time, end of the test indicator, current data in numerical form, and until change the data viewer. The user can visualize the input signal generated from the user parameters, and the output signals as the wave generated from the DAQ system and the height of the platform. Also, the user can select the FFT or moving average tabs to analyze the data.

The third part is composed of the emergency stop button. The user has 2 options to stop the test, the first is the software solution, and another one is the hardware option. It was proposed to bring redundancy to the security of the test procedure. The user can just turn off the energy button that stays on backward of the box to shut down the entire system. On the other hand, if it is preferable there is a software button, in which only the software stops.

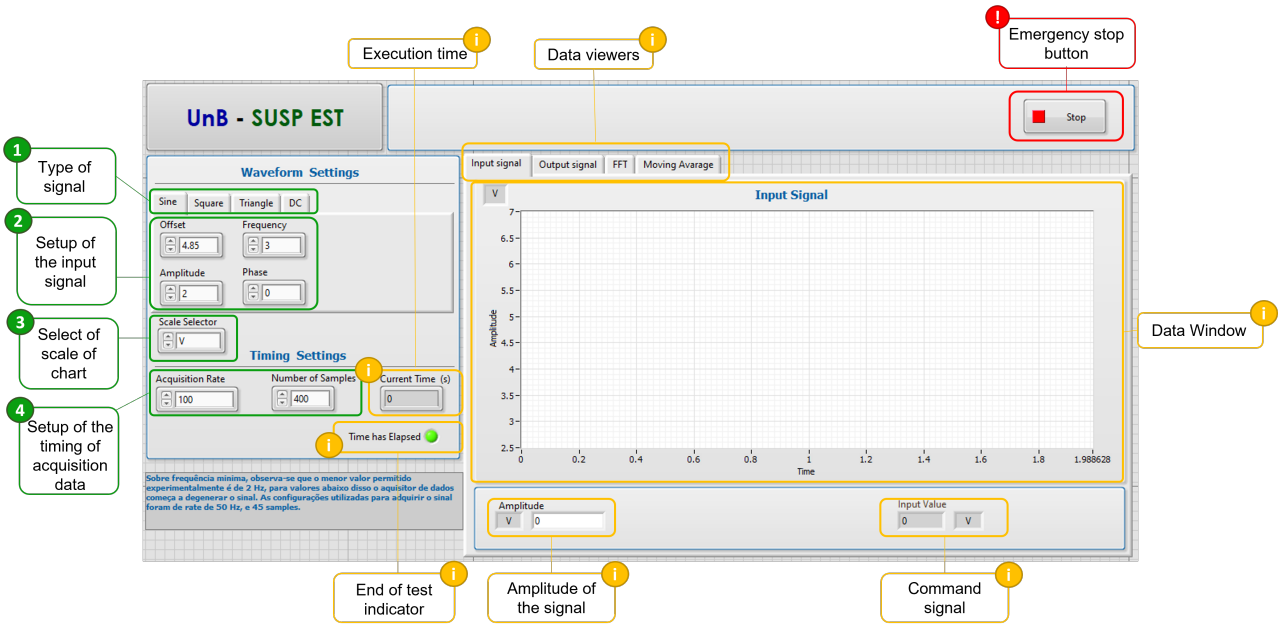

Figure 59 – LabVIEW user interface

6 Conclusion

Given the studies presented, it is observed the quarter-vehicle test rig is widely adopted in academia due to its lower costs and less manufacturing complexity compared to other test benches such as 4-post, 7-post, and 8-post rigs, being utilized to evaluate the suspension's durability, performance, and fatigue resistance. Additionally, it can also be applied to assess the global suspension parameters of a passenger car, being quite useful when compared to the characterization of isolated elements, to verify the influence of other components such as cushions, and control arms, that are also present in the suspension system.

Further, the state-space modeling provided a simplified view that describes a 1/4 car suspension that, together with the analysis of commercial suspension test benches, allowed the selection of the most relevant variables to be monitored and to raise the required instrumentation to be inserted in the test rig. Then, aiming to ensure the instrumentation inserted in the test bench was capable of obtaining the desired variables and guaranteeing the position feedback of the platform excitation experiments were also conducted to calibrate the measurement system e verify their experimental operating conditions.

Thus, it was noted that the test rig is not able to fully sweep the spectrum of frequencies recommended by the bibliography, due to the mechanical limitations of the excitation platform, as well as its displacement measurement sensor. Many experiments were carried out, to map the excitation platform transfer function to improve road profile generation software developed in previous work, however, the results were not promising. As it is a mechanical system, the points of connections require reform, because the test bench must support the vibration received.

As a consequence, open-loop software that allows monitoring data in real-time was deployed, ensuring to the user sets up tests through a friendly interface. Besides, the electrical system also presented more rugged, reliable, and safer to the quarter-car test rig user due to the improvements carried out, avoiding the user spending time making connections. Thus, the integration between electronics and software proved to be capable of promoting good usability.

Finally, the bench at the University of Brasilia showed to be quite important because it can permit the configuration of tests of different suspension geometries of passenger vehicles. Besides, its study helps to gather knowledge from different areas, such as vehicle dynamics, electronics, and programming, being an excellent precursor in the training of professionals who aim to learn about the technologies that can be applied in the automotive environment.

7 Future prospects

There are some points that can be improved that will bring more sophistication and security to the quality of the indoor test and reliability of the measured parameters, such as:

- Carry out the modeling of the plant of the system that generates the road profile to design a controller;
- Creating a mechanism that allows you to avoid the load cell does not have a load on it for long, to mitigate the effects of creep;
- Access some database with configurations of different suspension geometry and connects to the software developed in this work.

References

A&D. **Load cell QA**. Mar. 2022. https://aandd.jp/products/weighing/loadcell/introduction/load_cells_qa.html. Sections 4 and 8. Visited on: 13 Mar. 2022. Cit. on p. 34.

ANG, K. H.; CHONG, G.; LI, Y. PID control system analysis, design, and technology. **IEEE Transactions on Control Systems Technology**, v. 13, n. 4, p. 559–576, 2005. DOI: 10.1109/TCST.2005.847331. Cit. on p. 42.

ARC, A. R. C. **The ARC Shaker Rig**. http://www.arcindy.com/7-post.html. Visited on: 10 Apr. 2022. Cit. on p. 27.

BENTLEY, J. P. **Principles of Measurement Systems**. 4. ed. England: Pearson Education Limited, Jan. 2005. (10). ISBN 0130430285. Cit. on pp. 30, 31, 38.

BIMBA. **Pneumatic Application Reference Handbook**. 1. ed.: Bimba Manufacturing Company, 2022. v. 1. (1). Cit. on p. 40.

BRIEFS, T. **The Modern Industrial Workhorse: PID Controllers**. 2014. https://www.techbriefs.com/component/content/article/tb/pub/features/articles/20013. Visited on: 8 Feb. 2023. Cit. on p. 42.

COLLIMATOR. **Designing a Car Suspension System**. Feb. 2023. https://www.collimator.ai/tutorials/car-suspension-design. Visited on: 25 Feb. 2023. Cit. on p. 18.

COMÉRCIO S.A, C. I. e. **iCLAMPER Energia 5**. 2021. https://s3.amazonaws.com/nerit-cms/clamper/file/fil_0049-FT_iCLAMPER%20Energia%205_05. Visited on: 2 Mar. 2023. Cit. on p. 61.

CONNECTIVITY, T. **Accelerometer Types**. 2022. https://www.te.com/usa-en/industries/sensor-solutions/insights/types-of-accelerometers.html#chapter-5-dl. Visited on: 20 Apr. 2022. Cit. on p. 37.

DIXON, J. C. **The Shock Absorber Handbook**. 2. ed. West Sussex PO19 8SQ, England: Professional Engineering Publishing Ltd, John Wiley, and Sons, Ltd., 2007. ISBN 978-0-470-51020-9. Cit. on pp. 30, 35.

ELPROCUS. **What is an IR Sensor : Circuit Diagram Its Working**. 2022. https://www.elprocus.com/infrared-ir-sensor-circuit-and-working/. Visited on: 26 Dec. 2022. Cit. on p. 32.

ENGINEERING, R. **Seven-post rigs Shaking down the best in suspension testing tech**. June 2018. https://www.servotestsystems.com/media/attachments/2020/04/17/reprint_-_racecar_engineering_june_july_2018.pdf. Visited on: 10 Apr. 2022. Cit. on p. 26.

FESTO. **Proportional directional control valves MPYE**. Oct. 2022. Cit. on pp. 41, 53.

FLOW, N. **What is the Difference between pneumatics and hydraulics?** 2021. https://www.nexflow.com/blog/difference-between-pneumatics-and-hydraulics/. Visited on: 29 Jan. 2023. Cit. on p. 38.

GAGLIANO, C. J.; GOBBI, M.; MASTINU, G.; PENNATI, M. Indoor/Outdoor Testing of a Passenger Car Suspension for Vibration and Harshness Analysis. **SAE International**, v. 5, n. 2, p. 937–948, 2012. Cit. on p. 17.

GEFRAN. **APZ12 Corpo cilíndrico 1/2 polegada**. Mar. 2022. https://www.gefran.com/pt/br/download/3215/attachment/en. Visited on: 14 Mar. 2022. Cit. on p. 31.

GILLESPIE, T. **Fundamentals of Vehicle Dynamics**. Society of Automotive Engineers, 1992. (Premiere Series Bks). ISBN 9781560911999. Cit. on p. 45.

GRIFFIN, M. **Handbook of Human Vibration**. ACADEMIC PRESS, 1990. ISBN 0-12-303040-4. Cit. on p. 23.

HAMED, M.; TESFA, B.; GU, F.; BALL, A. A study of the suspension system for the diagnosis of dynamic characteristics. In: 2014 20th International Conference on Automation and Computing. 2014. P. 152–157. DOI: 10.1109/IConAC.2014.6935478. Cit. on p. 29.

HASBOLLAH, R. **Main Parts of a Car: The Different Car Systems How They Relate to Each Other**. 2021. https://carpart.com.au/blog/masterpiece/major-parts-of-a-car-the-different-car-systems-how-they-relate-to-each-other. Visited on: 2 May 2022. Cit. on p. 17.

HBM. **loadcell group teaser**. Mar. 2022. https://www.hbm.com/fileadmin/mediapool/images/products/sensors/load-cells/wei-loadcell-group-teaser.png. Visited on: 13 Mar. 2022. Cit. on p. 34.

HOFFMANN, K. **An Introduction to Measurements using Strain Gages**. 1. ed. Darmstadt: Hottinger Baldwin Messtechnik GmbH, 1989. v. 1. (1). Cit. on pp. 33, 34.

INSTRUMENTS, N. **Chassi CompactDAQ**. 2022. https://www.ni.com/pt-br/shop/hardware/products/compactdaq-chassis.html. Visited on: 5 May 2022. Cit. on p. 52.

INSTRUMENTS, N. **NI 9219 Getting Started Guide**. 2017. https://www.ni.com/pdf/manuals/377223a.pdf. Visited on: 5 May 2022. Cit. on pp. 50, 52, 53, 59.

INSTRUMENTS, N. **NI 9264 Getting Started Guide**. 2016. https://www.ni.com/pdf/manuals/374404g.pdf. Visited on: 5 May 2022. Cit. on p. 51.

INSTRUMENTS, N. **NI cDAQ-9172 User Guide and Specifications**. June 2008. http://edge.rit.edu/edge/P16371/public/Systems%20Level%20Design%20Documents/NI9712.pdf. Visited on: 2 Sept. 2022. Cit. on p. 51.

INSTRUMENTS, N. **NI-9234 Specifications**. 2021. https://www.ni.com/docs/en-US/bundle/ni-9234-specs/page/overview.html. Visited on: 2 Mar. 2023. Cit. on p. 51.

INSTRUMENTS, N. **Strain Gauge Measurement – A Tutorial**. 1998. http://elektron.pol.lublin.pl/elekp/ap_notes/ni_an078_strain_gauge_meas.pdf. Cit. on p. 33.

IRWIN, J. D.; NELMS, R. M. **Basic Engineering Circuit Analysis**. 10. ed. United States: John Wiley Sons, Inc, July 2011. ISBN 978-0-470-63322-9. Cit. on pp. 30, 35.

JOIE, J. L. **7 Post Shaker Rig vs. KC Rig**. Feb. 2023. https://www.morsemeasurements.com/kc-vs-shaker-rig/. Visited on: 25 Feb. 2023. Cit. on p. 18.

KAMATH, A. **Signal and Power Isolation Considerations for Compact, Efficient Analog Input Modules**. 2020. Systems Engineer, Isolation Products, Interface Group. Cit. on p. 50.

KOCH, G.; PELLEGRINI, E.; SPIRK, S.; LOHMANN, B. **Design and Modeling of a Quarter-Vehicle Test Rig for Active Suspension Control**. July 2010. Cit. on p. 26.

KW. **KW 7-post driving dynamics test**. Feb. 2023. https://www.kwsuspensions.co.uk/technology/kw_7_post. Visited on: 25 Feb. 2023. Cit. on p. 18.

LANGDON, J. **Design and Adaptive Control of a Lab-based, Tire-coupled, Quarter-car Suspension Test Rig for the Accurate Re-creation of Vehicle Response**. Jan. 2007. MA thesis – Virginia Polytechnic Institute, Danville VA. An optional note. Cit. on p. 18.

LEÓN-VARGAS, F.; GARELLI, F.; ZAPATEIRO, M. Limiting vertical acceleration for ride comfort in active suspension systems. **Journal of Systems and Control Engineering**, p. 1–10, 2017. Cit. on p. 24.

MENG, D.; TAO, G.; CHEN, J.; BAN, W. Modeling of a Pneumatic System for High-Accuracy Position Control. **IEEE**, p. 505–510, 2011. Cit. on p. 42.

METROLOG. **ACT LVDT Displacement Transducer**. Aug. 2016. https://www.metrolog.net/files/act_en_metrolog.pdf. Visited on: 14 Mar. 2022. Cit. on p. 31.

MICHELIN. **An Unknown Object The Tire, Functions of the Tire**. https://thetiredigest.michelin.com/an-unknown-object-the-tire-functions-of-the-tire. Visited on: 13 Apr. 2022. Cit. on p. 22.

MITRA, A. C.; R., K. G.; SONI, T.; BANERJEE, N. Design of Experiments For Optmization Of Automotive Suspension System Using Quarter Car Test Rig. **12th International Conference on Vibration Problems**, p. 1102–1109, 2015. Cit. on p. 24.

MODELON. **Multi-body Vehicle Dynamics: Efficient Suspension Design in Modelon Impactv**. Feb. 2023. https://modelon.com/blog/multibody-vehicle-dynamics-suspension-design-in-modelon-impact/. Visited on: 25 Feb. 2023. Cit. on p. 18.

MTS. **Suspension Test System for Evaluating Performance, Durability**. 2011. https://corp.mts.com/cs/groups/public/documents/library/dev_002223.pdf. Visited on: 10 Apr. 2022. Cit. on p. 26.

NISE, N. **Control Systems Engineering, Sixth**. 6. ed.: John Wiley & Sons, Incorporated, 2011. (Instrumentation and controls series). ISBN 9781118138168. Cit. on p. 28.

NOTES, E. **What is Data Acquisition**. 2022. https://www.electronics-notes.com/articles/test-methods/data-acquisition-daq/understanding-data-acquisition.php. Visited on: 20 Apr. 2022. Cit. on p. 43.

PATHARE, Y. S. Design And Development Of Quarter Car Suspension Test Rig Model And It's Simulation. **International Journal of Engineering Science Advanced Technology**, v. 4, p. 157–170, Nov. 2014. Cit. on p. 27.

PAVLOV, N. Influence of shock absorber temperature on vehicle ride comfort and road holding. **MATEC Web of Conferences**, v. 133, n. 02006, p. 3–6, Nov. 2017. Cit. on p. 30.

RAJAMANI, R. **Vehicle Dynamics and Control**. 1. ed.: Springer, June 2006. ISBN 9780387263960. Cit. on pp. 28, 29, 45.

RESEARCH, P. M. **Automotive Suspension Systems Market**. Apr. 2021. https://www.persistencemarketresearch.com/market-research/automotive-suspension-systems-market.asp. Visited on: 5 May 2022. Cit. on p. 17.

RILL, G. **Road Vehicle Dynamics: Fundamentals and Modeling**. 1. ed.: CRC Press, 2011. ISBN 1439838984. Cit. on pp. 21–23.

SAE. **SURFACE VEHICLE RECOMMENDED PRACTICE - J1574-1**. Jan. 2018. P. 82–87. Cit. on p. 31.

SALEM, M. H. H. Investigation of a non-linear suspension in a quarter car model. In. Cit. on pp. 18, 25.

SERVOTEST. **7- 8-post advanced ride simulators for performance race vehicle testing**. Feb. 2023. https://www.servotestsystems.com/7-8-post-advanced-ride-simulators-for-performance-race-vehicle-testing. Visited on: 25 Feb. 2023. Cit. on p. 18.

TAMESON. **Pneumatic Cylinders - A Technical Guide**. 2022. https://tameson.com/pneumatic-cylinders.html. Visited on: 19 Apr. 2022. Cit. on p. 39.

TEXAS, I. **Temperature Sensing, Industrial Automation Solutions**. 2013. Cit. on p. 36.

TRUCK, T. A. .⟨. **WHEN TO REPLACE SUSPENSION PARTS**. 2020. https://www.tlcautotruck.com/blog/when-to-replace-suspension-parts/. Visited on: 8 Apr. 2022. Cit. on p. 21.

VETTURI, D.; MAGALINI, A. Road profile excitation on a vehicle measurements and indoor testing using a four-post rig, 2002. Cit. on p. 17.

WOJCIK, B. **The Difference Between Proportional vs. Directional vs. Servo Valves**. 2022. https://www.qualityhydraulics.com/blog/valves/what-proportional-valve. Visited on: 23 Jan. 2023. Cit. on p. 40.

WU, J. **A Basic Guide to Thermocouple Measurements**. July 2018. Application Report SBAA274. Cit. on pp. 36, 37.

WULING. **9 Car Suspension Components and Their Functions**. Mar. 2021. https://wuling.id/en/blog/autotips/9-car-suspension-components-and-their-functions/. Visited on: 13 Apr. 2022. Cit. on p. 21.

AL-ZUGHAIBI, A.; XUE, Y.; GROSVENOR, R. A New Insight into Modeling Passive Suspension Real Test Rig System with Considering Nonlinear Friction Forces. **Journal of Automobile Engineering**, p. 2257–2266, 2019. Cit. on p. 25.

Annex

ANNEX A – Fractional frequencies experiment results

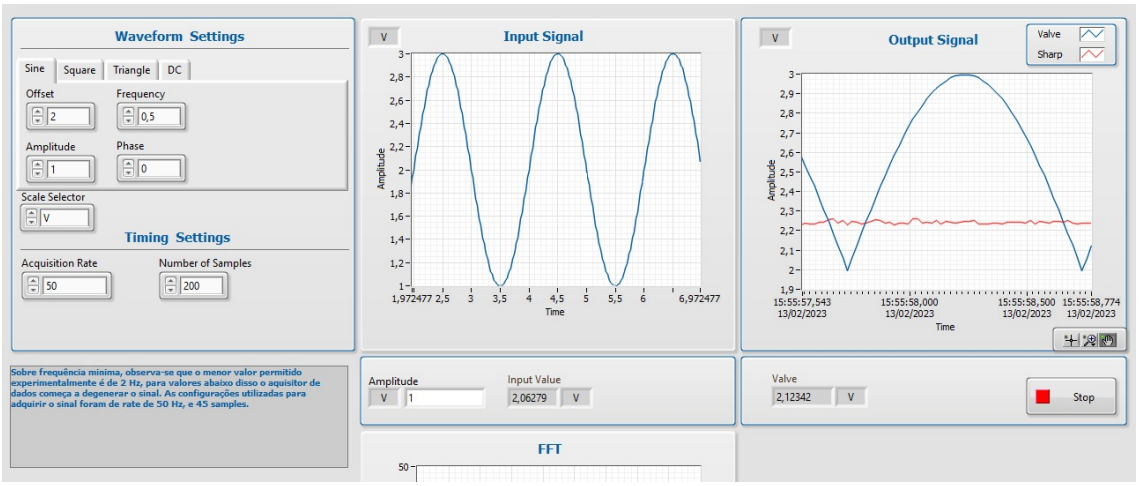

Figure 60 – 0.5 Hz sinusoidal wave

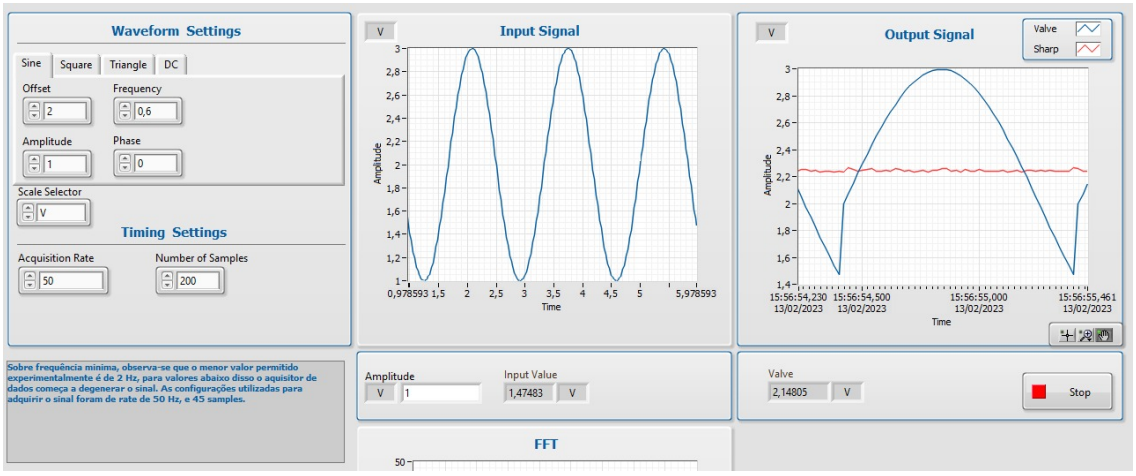

Figure 61 – 0.6 Hz sinusoidal wave

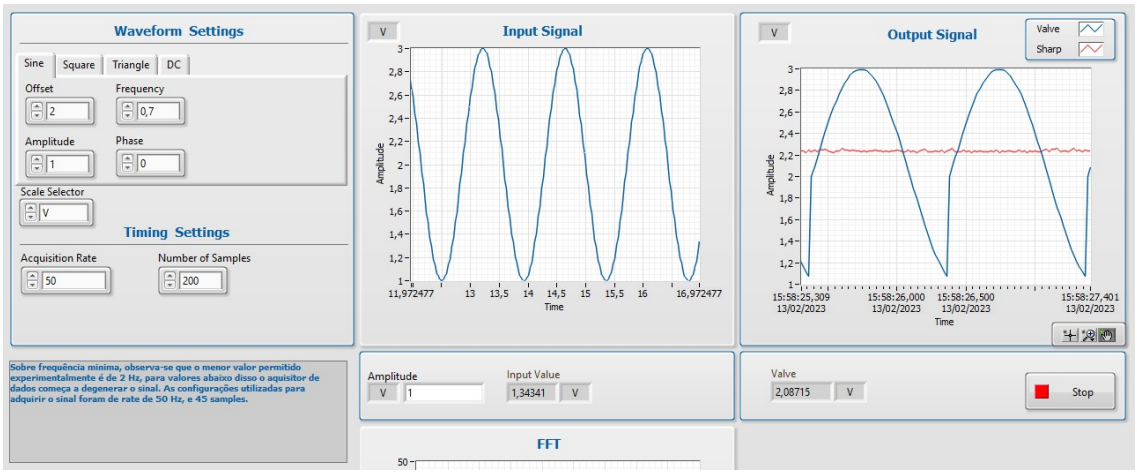

Figure 62 – 0.7 Hz sinusoidal wave

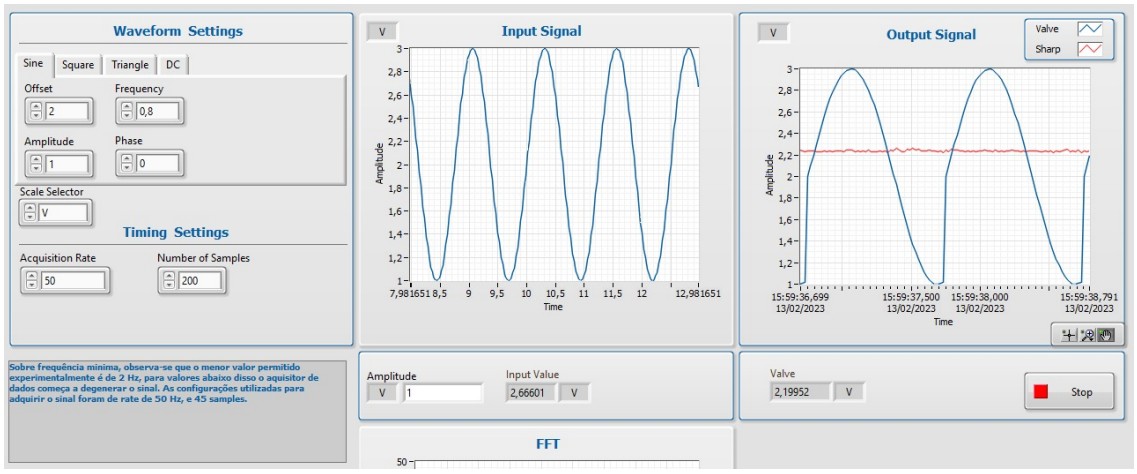

Figure 63 – 0.8 Hz sinusoidal wave

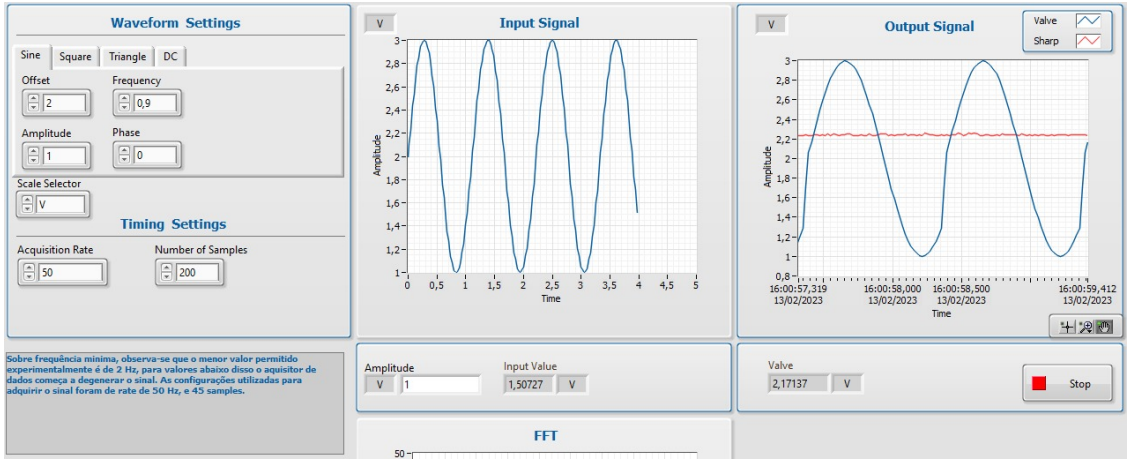

Figure 64 – 0.9 Hz sinusoidal wave

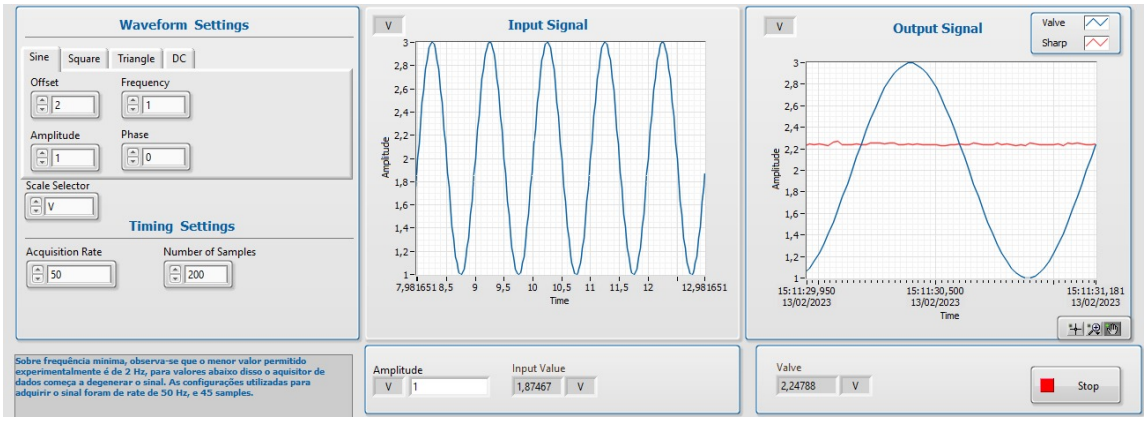

Figure 65 – 1 Hz sinusoidal wave

ANNEX B – The complete range of frequency experiment results

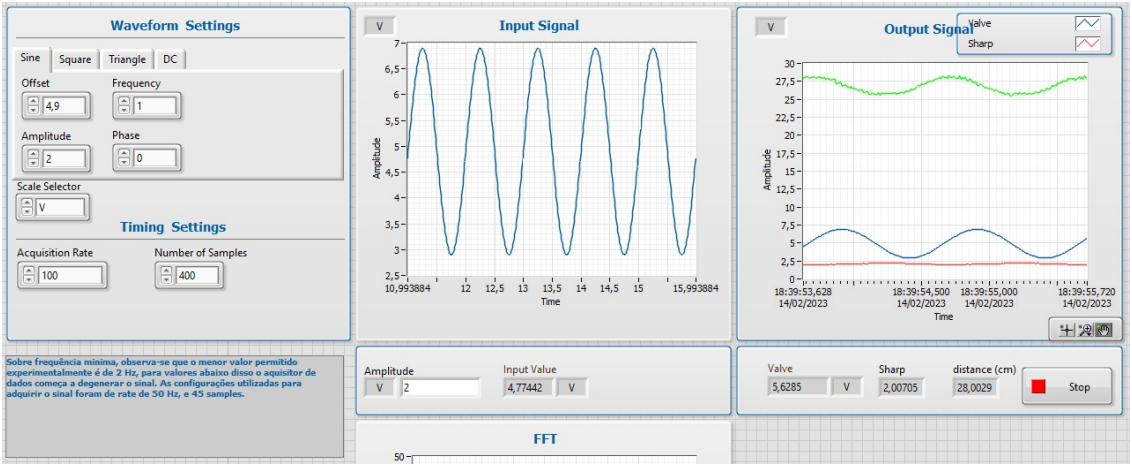

Figure 66 – Input signal of 1Hz and 400 samples

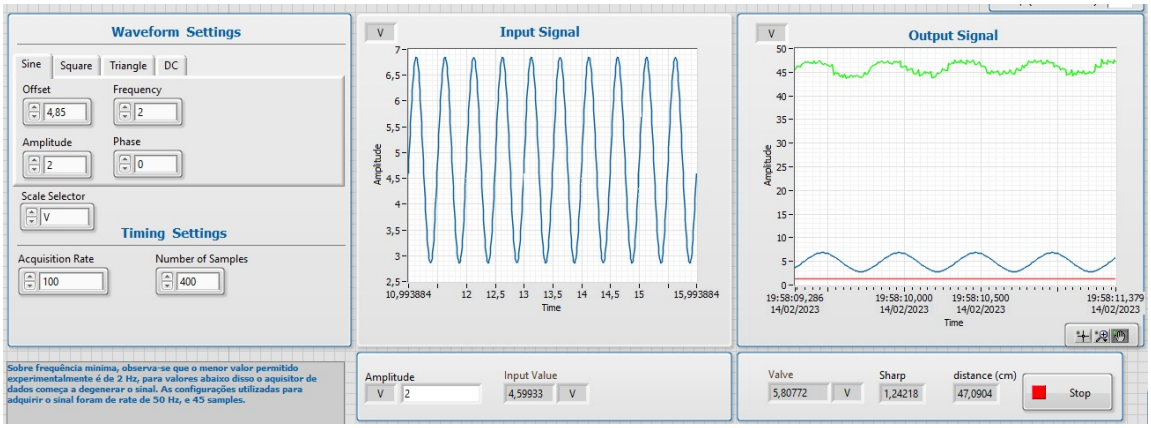

Figure 67 – Input signal of 2Hz and 400 samples

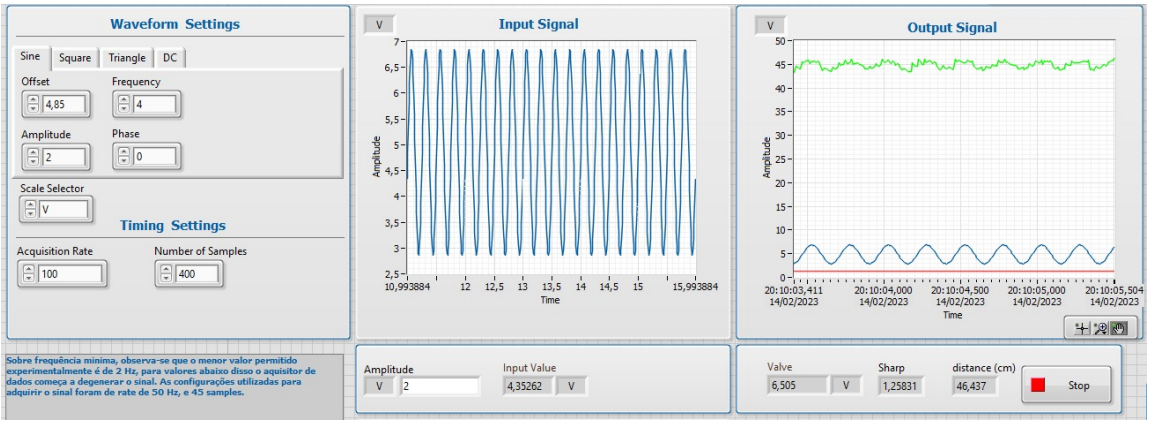

Figure 68 – Input signal of 4Hz and 400 samples

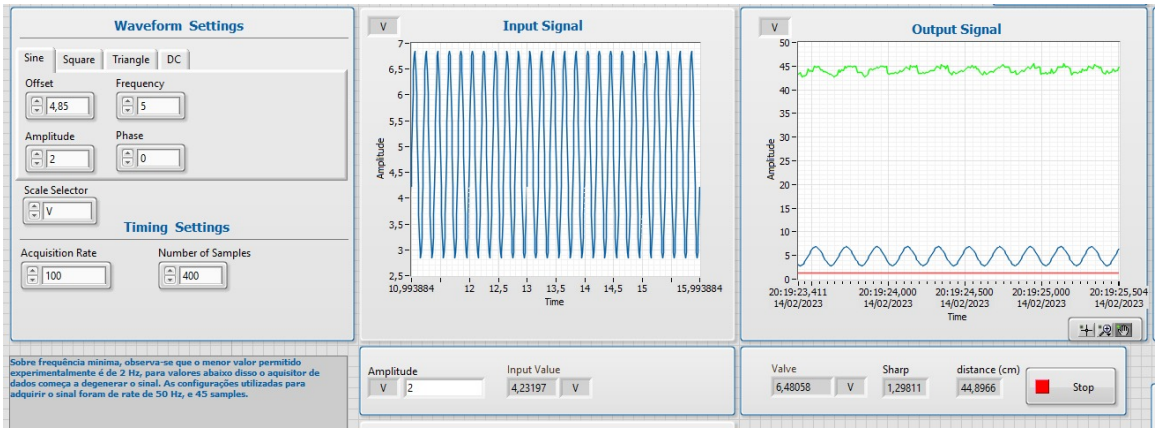

Figure 69 – Input signal of 5Hz and 400 samples

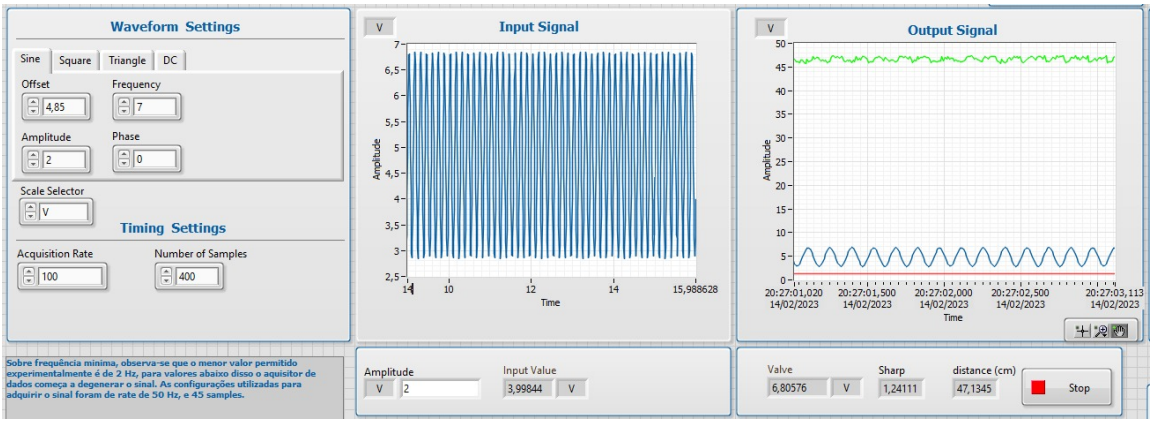

Figure 70 – Input signal of 7Hz and 400 samples

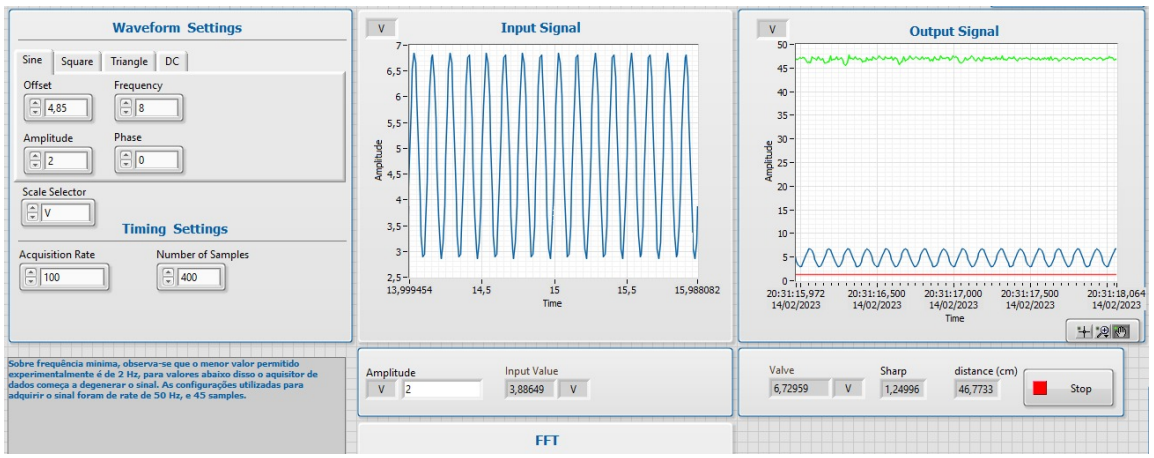

Figure 71 – Input signal of 8Hz and 400 samples

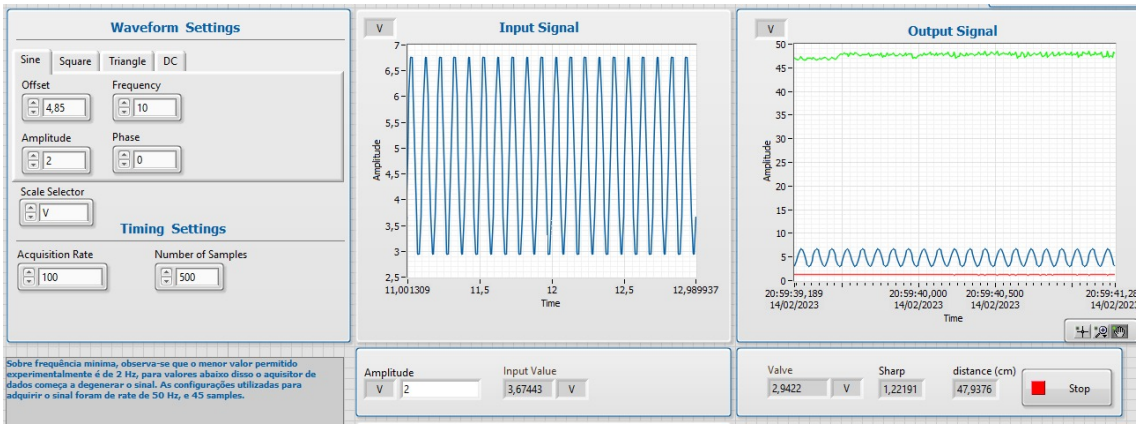

Figure 72 – Input signal of 10Hz and 400 samples